Radiation Laboratory
Electrical and Computer Engineering Department
The University of Michigan
Ann Arbor, Michigan 48104

EFFECT OF AN INTRUDER ON A SECURITY SYSTEM

by

Thomas B.A. Senior

Prepared for

Omni Spectra, Inc.
24600 Hallwood Court
Farmington, Michigan 48024

July 1975

348330-1-F = RL-2533

EFFECT OF AN INTRUDER ON A SECURITY SYSTEM

The purpose of this study was to develop a theoretical model simulating the effect of a man in various positions relative to one of the Omni-spectra microwave security systems. To guide the development of the model and to provide information with which to judge the effectiveness of the simulation, data were supplied showing the signal measured at the receiving antenna under carefully controlled conditions. The conditions governing these experiments are discussed in Chapter 1 and selected data are presented in Chapter 3. Chapter 2 is concerned with the theoretical modelling of the scattering situation. Formulas appropriate to the near-forward scattering situation for a man-like object are derived and the resulting expression for the perturbed signal at the receiving antenna reproduces all of the key features observed in the measured data. The expression also satisfies the other requirements of "physical meangfulness" and wide applicability, and a program for the computation of the received signal is listed in the Appendix.

1. Preliminary Considerations

The system consists of two identical 8-inch diameter center fed dishes a horizontal distance d apart and mounted with their (phase) centers at heights z_1 and z_2 above the ground. The frequency used is 10.525 GHz, implying a wavelength $\lambda = 1.1214$ inches, and the transmitted field is horizontally polarized.

The measured polar diagram of a dish is shown in Fig. 1. The main lobe is rather clean with a width $\pm 9^{o}$ at the -10 dB level, but since the diagram is not quite centered on the 180^{o} line of the chart, we have transcribed the lobe, centering it and then averaging the two sides. The resulting voltage polar diagram $P(\alpha)$ plotted on a linear scale is shown in Fig. 2. A numerical fit is provided by the formula

$$P(\alpha) = (1 + 9.04 \times 10^{-13} \alpha^{10}) \exp(-0.0114\, \alpha^{2}) \qquad (1)$$

where α is measured in degrees, and this has been used in all of our numerical work, even in those cases where the angles involved exceed 18^{o}. Although Eq. (1)

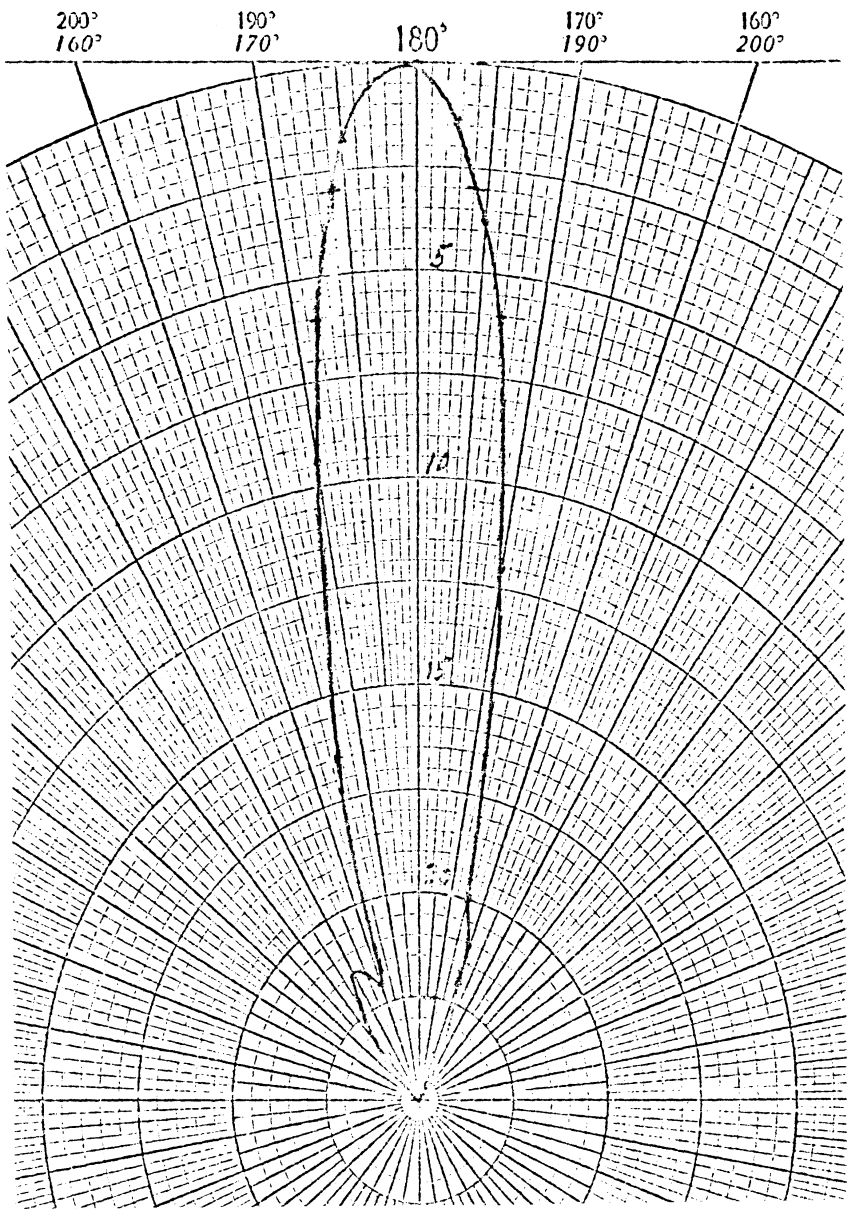

Fig. 1: Measured antenna polar diagram.

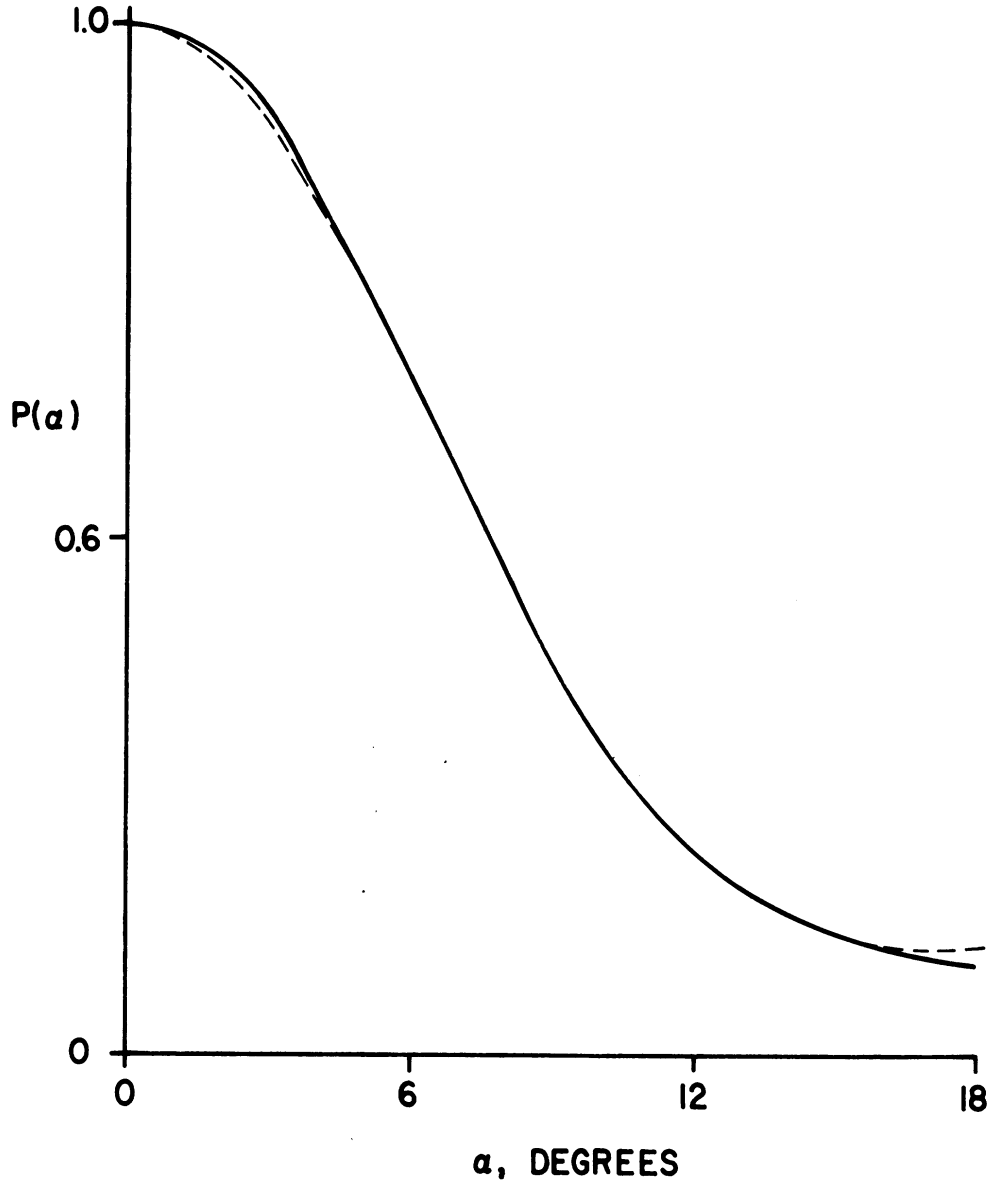

Fig. 2: Voltage polar diagram: (——) average measured, (----) analytical simulation, eq. (1).

does not, of course, reproduce the side lobes of the antenna pattern, their actual contribution in all cases of interest to us is so small as to be insignificant.

For the test data supplied to us, the measurements were carried out in a garage having a rather flat concrete floor with the antennas 100 ft apart. In most cases $z_1 = z_2 = 40$ inches although some data were obtained with measured heights lower than this. In examining the role played by the ground under these circumstances, we first remark that since the range and heights involved are all large compared with the wavelength, we would expect some form of ray theory to be applicable. On the assumption of a smooth planar ground, the angle of incidence of a ray specularly reflected to the receiving antenna is small indeed, suggesting that the voltage reflection coefficient of the ground for horizontal polarization will be close to -1. Since the angle to grazing is

$$\theta = \tan^{-1} \frac{z_1 + z_2}{d} \quad ,$$

we have, for example,

$$z_1 = z_2 = 40 \text{ in.} : \qquad \theta = 3.814^{\circ}$$

and

$$z_1 = z_2 = 38 \text{ in.} : \qquad \theta = 3.624^{\circ} .$$

The Fresnel reflection coefficient for an incident plane wave polarized perpendicular to the plane of incidence is

$$\rho(\theta) = - \frac{\sqrt{\epsilon^2 - \cos^2\theta} - \sin\theta}{\sqrt{\epsilon^2 - \cos^2\theta} + \sin\theta} \qquad (2)$$

(Stratton, 1941; p. 493) where ϵ is the complex permittivity of the ground material whose permeability has been assumed equal to that of free space. From waveguide measurements of representative samples of concrete, Cosgriff et al. (1960; p. 14) report that at X-band frequencies $\epsilon = 6.5 + i1.5$, and using this and the average value $\theta = 3.75^{\circ}$, Eq. (2) gives

$$|\rho| = 0.9472 \ , \qquad \arg\rho = 180.4^{\circ} .$$

Since the results are relatively insensitive to the precise value of θ, it would seem sufficient to choose

$$\rho = 0.95\, e^{i\pi} \tag{3}$$

in simulating the measured data.

The point of specular reflection is that for minimum path distance from the transmitter to the receiver via the surface of the earth. It is also the stationary phase (or saddle) point of a physical optics integral expression for the field scattered by the ground in the direction of the receiving antenna, and though it is true that the dominant contribution to the integral is provided by the surface area in the immediate vicinity of this point, it is also true that for nonzero λ there is some contribution from the surrounding area. This leads to the concept of Fresnel zones, with the first zone being the area responsible for the return.

If x, y are Cartesian coordinates in the plane of the ground referred to an origin at the base of the transmitter, the distance from the transmitter to an arbitrary point on the ground is

$$R_1' = \sqrt{x^2 + y^2 + z_1^2}$$

(see Fig. 3), and for $x \gg \sqrt{y^2 + z_1^2}$,

$$R_1' \simeq x + \frac{1}{2x}(y^2 + z_1^2) .$$

The distance from the receiver is similarly

$$R_2' = \sqrt{(d-x)^2 + y^2 + z_2^2} \simeq d - x + \frac{1}{2(d-x)}(y^2 + z_2^2)$$

and if we define the first Fresnel zone as the surface region where the electrical distance (or phase) exceeds the minimum by no more than $\pi/4$, the boundary of the zone is given by

$$k(R_1' + R_2') = k(R_1 + R_2) = \pi/4$$

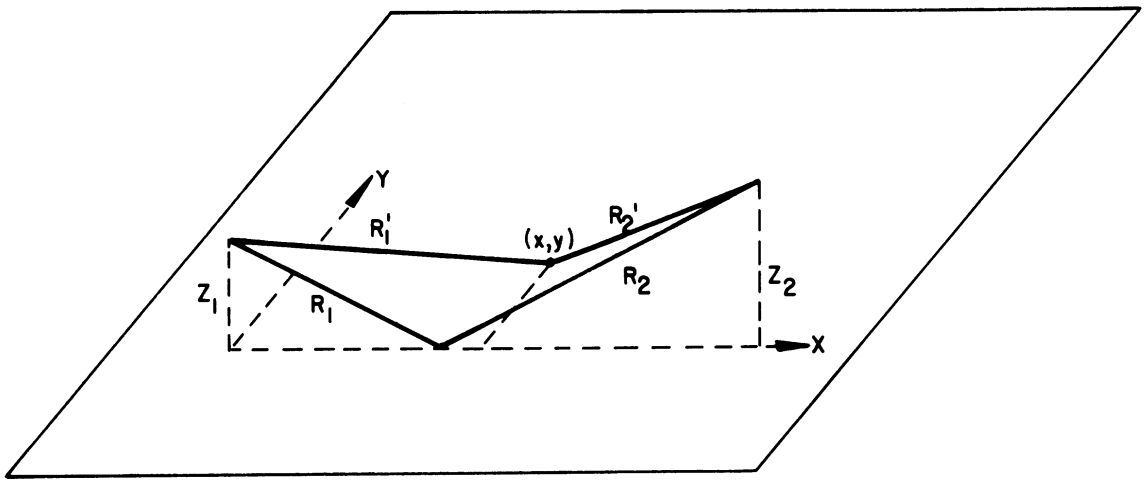

Fig. 3: Geometry for Fresnel zone calculation.

Since

$$R_1 + R_2 \simeq d + \frac{1}{2d}(z_1 + z_2)^2$$

it follows that in the particular case $z_2 = z_1$ the boundary of the zone is

$$\frac{y^2 + z_1^2}{x(d-x)} = (2z_1/d)^2 + \frac{\lambda}{4d}$$

and when $z_1 = 40$ inches,

$$\left(\frac{y}{0.7642}\right)^2 + \left(\frac{x-50}{11.17}\right)^2 = 1 \tag{4}$$

where all dimensions are in feet. Equation (4) is an ellipse of semi-axes 11.17 and 0.7642 ft. centered on the point of specular reflection, and is plotted in Fig. 4. If we enlarge the zone to correspond to phase differences of up to $\pi/2$ (path length up to $\lambda/4$), Eq. (4) is replaced by

$$\left(\frac{y}{1.081}\right)^2 + \left(\frac{x-50}{15.42}\right)^2 = 1 \tag{5}$$

and this curve is also plotted in Fig. 4. With either definition, the zone is a very slender ellipse and will be substantially blotted out by a narrow object resting on the ground in the boresight plane $y = 0$.

In addition, the ground illumination produced by the transmitter is a variable function of position throughout the zone. If the radiated field is taken to be

$$E = P(\alpha)\frac{e^{ikR}}{R} \tag{6}$$

where α is measured relative to a horizontal line in the boresight plane, the ground illumination is

$$\left|E(x, y)\right| = \frac{P(\alpha)}{R_1'} \tag{7}$$

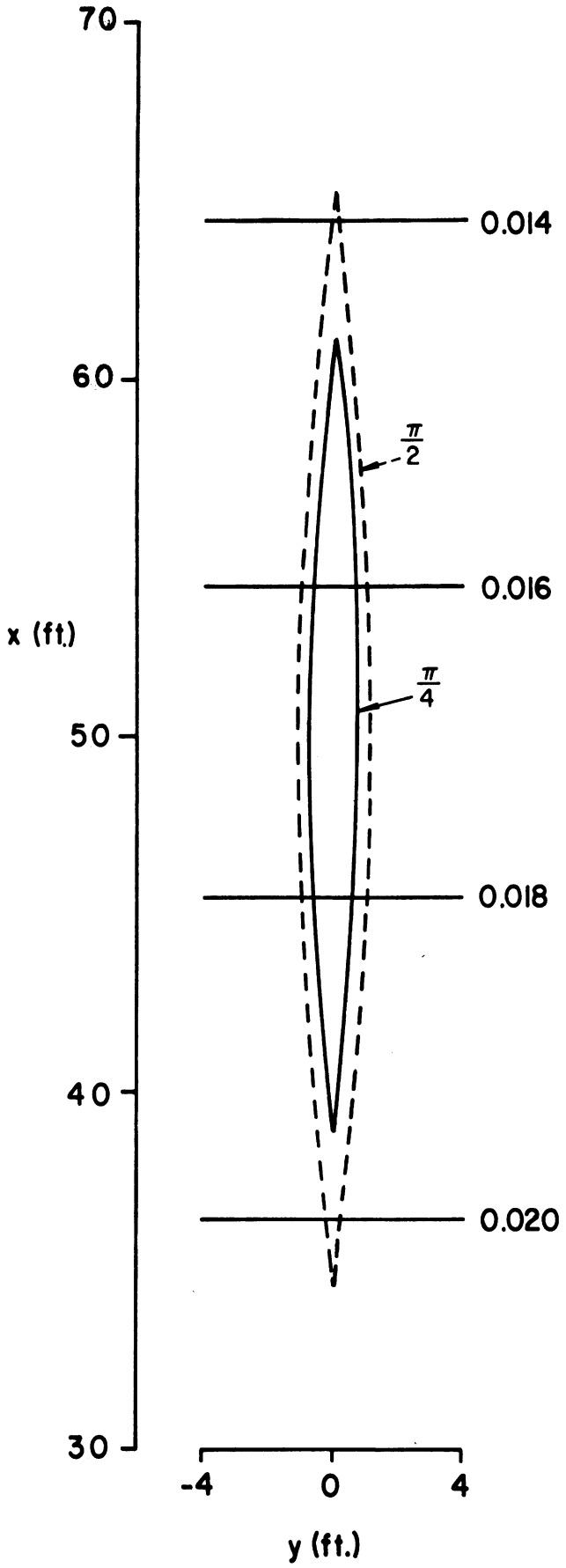

Fig. 4: Fresnel zones and their illumination.

with $\alpha = \tan^{-1}\left\{\frac{1}{x}(y^2+z_1^2)^{1/2}\right\}$. The decrease with distance is partially offset by the polar diagram of the transmitter, and some "curves" of constant $|E|$ are superimposed on Fig. 4. It is seen that the illumination varies very slowly throughout the Fresnel zone and is not in itself a factor which significantly affects the region contributing to the ground return.

In contrast, any roughness that the surface possesses could be an important factor, and affect the region which contributes through the random phasing introduced. Cosgriff et al. (1960) have examined the rms roughness of representative samples of concrete roadway and found it to be approximately 0.015 cm (= 0.0063 inches). This is much less than the wavelength and indicates that smooth concrete should act as a coherent specular reflector at X-band. They also measured the surface correlation as a function of distance (p. 14) and the scattering as a function of the angle from the specular direction, out of the plane of incidence as well as in it. These data confirm the specular nature of the scattering and show that the roughness is too small to have any noticeable effect on the reflected field.

For at least a concrete surface it now seems adequate to simulate the presence of a ground by a single ray reflection, allowing us to replace the ground in favor of an image transmitter localized at the geometric image of the real transmitter in the ground and having a relative strength determined by the Fresnel reflection coefficient ρ. This is, of course, an approximation for any ground other than a perfectly conducting one, but is reasonable for the types of smoothed surface near which the system is likely to be installed. More to the point, however, the approximation is essential to obtain any usable simulation of the effect of an intruder.

It is now a simple matter to determine the received voltage in the absence of any perturbation. If the free space field of the transmitting antenna is that of Eq. (7), the "direct" field at the receiving antenna is obtained by giving α the value δ, where the angle δ is shown in Fig. 5. The corresponding voltage is

$$\left\{P(\delta)\right\}^2 \frac{e^{ikR}}{R}$$

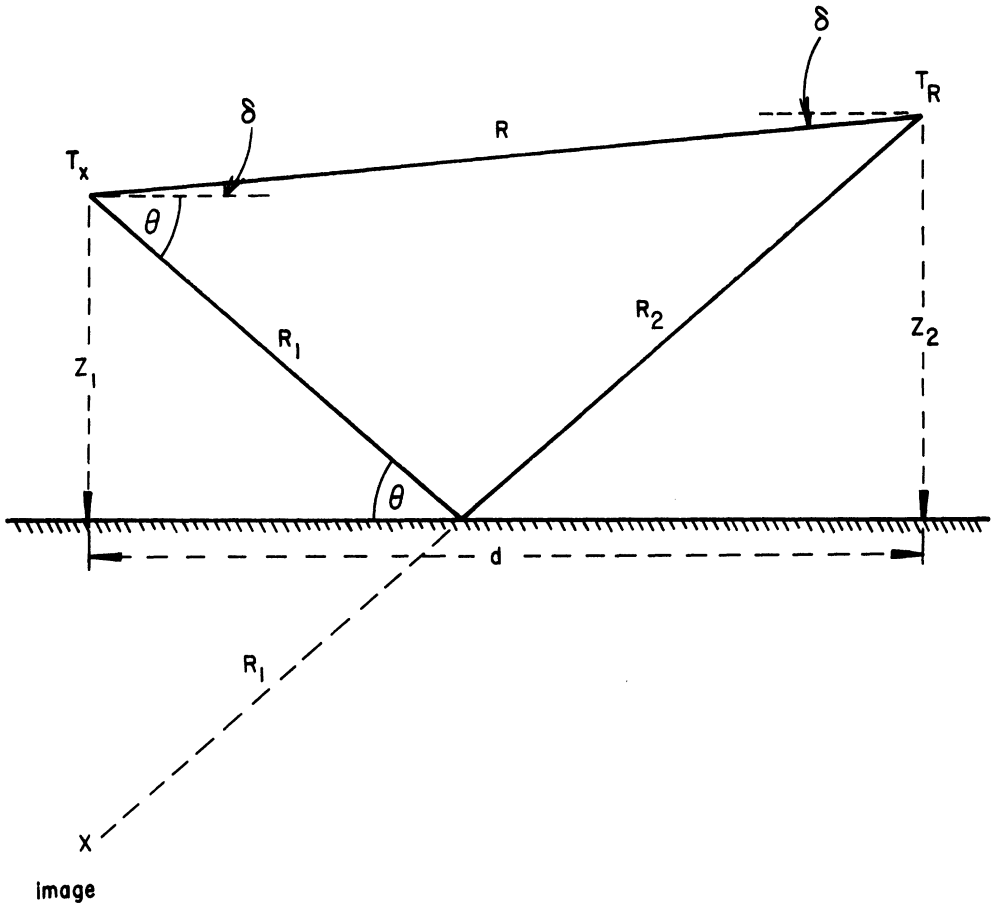

Fig. 5: Ray geometry.

provided both antennas are looking horizontally so that their polar diagrams are symmetric about the zero angle. The field which reaches the receiving antenna after reflection from the smooth ground is represented by the field of an image transmitter of strength ρ, and its contribution is

$$\rho(\theta)\left\{P(\theta)\right\}^2 \frac{\exp\left\{ik(R_1+R_2)\right\}}{R_1+R_2} \quad ,$$

leading to the net voltage

$$V = \left\{P(\delta)\right\}^2 \frac{e^{ikR}}{R}\left[1+\rho(\theta)\left\{\frac{P(\theta)}{P(\delta)}\right\}^2 \frac{R}{R_1+R_2}\exp\left\{ik(R_1+R_2-R)\right\}\right] .$$

For $d \gg z_1+z_2$,

$$R_1+R_2 = \left\{d^2+(z_1+z_2)^2\right\}^{1/2} \simeq d+\frac{1}{2d}(z_1+z_2)^2$$

and

$$R = \left\{d^2+(z_1-z_2)^2\right\}^{1/2} \simeq d+\frac{1}{2d}(z_1-z_2)^2 \quad ,$$

implying

$$\frac{R}{R_1+R_2} \simeq 1$$

and

$$R_1+R_2-R \simeq \frac{2z_1z_2}{d} \quad .$$

With z_1 near 40 inches and z_2 in the range 30 to 45 inches approx., $P(\delta)$ differs from unity by less than 0.5 percent and $P(\theta)$ varies by no more than two percent about a mean value of 0.85. It is therefore sufficient to ignore the variation of $P(\theta)/P(\delta)$ for such changes in height, and to an adequate approximation

$$V = \left\{P(\delta)\right\}^2 \frac{e^{ikR}}{R} A(z_1, z_2) \tag{8}$$

where

$$A(z_1, z_2) = 1 + 0.85|\rho| \exp\left\{i(2kz_1z_2/d + \arg\rho)\right\} \quad . \tag{9}$$

If either z_1 or z_2 is fixed, the received voltage will oscillate as a function of the other height, corresponding to constructive and destructive interference between the direct and ground-reflected signals. It is reported that for $z_1 = z_2 = 40$ inches and $d = 100$ ft the received signal was a maximum, but if this was so the maximum must have been the third one above the surface, and Eq. (9) then implies that $\arg\rho = 224.9^o$. This is highly improbable and quite at variance with the expected value based on the constitutive parameters of concrete. If, instead, we use the value of $\arg\rho$ given in Eq. (3), A is a maximum if $z_1 = z_2 = 41.01$ inches, and the next lower maximum is at 31.77 inches. Although it is possible that the discrepancy is due to an error in the height measurement of the antennas, or even to a displacement of the phase center of each dish from its geometrical center, a more likely explanation is that the concrete floor was slightly concave. Were it one inch lower at the center of the range, perhaps even intentionally so for drainage purposes, the antenna heights relative to the reflection point of the ground-reflected ray would exceed the measured heights by this amount, thereby accounting for the discrepancy. In the absence of information to the contrary, this explanation will be accepted, and henceforth it is assumed that the "true" heights of the transmitting and receiving antennas exceed their measured values by an inch.

For the reflection coefficient (3) of concrete for angles close to grazing, Eq. (9) becomes

$$A(z_1, z_2) = 1 - 0.8075 \exp\left(i\pi \frac{4z_1z_2}{\lambda d}\right) \tag{10}$$

and it is a trivial task to compute this as a function of z_1 and/or z_2. Figure 6 shows the variation of $\left|A(z_1, z_1)\right|$ for $0 \leq z_1 \leq 45$ inches, from which it is evident

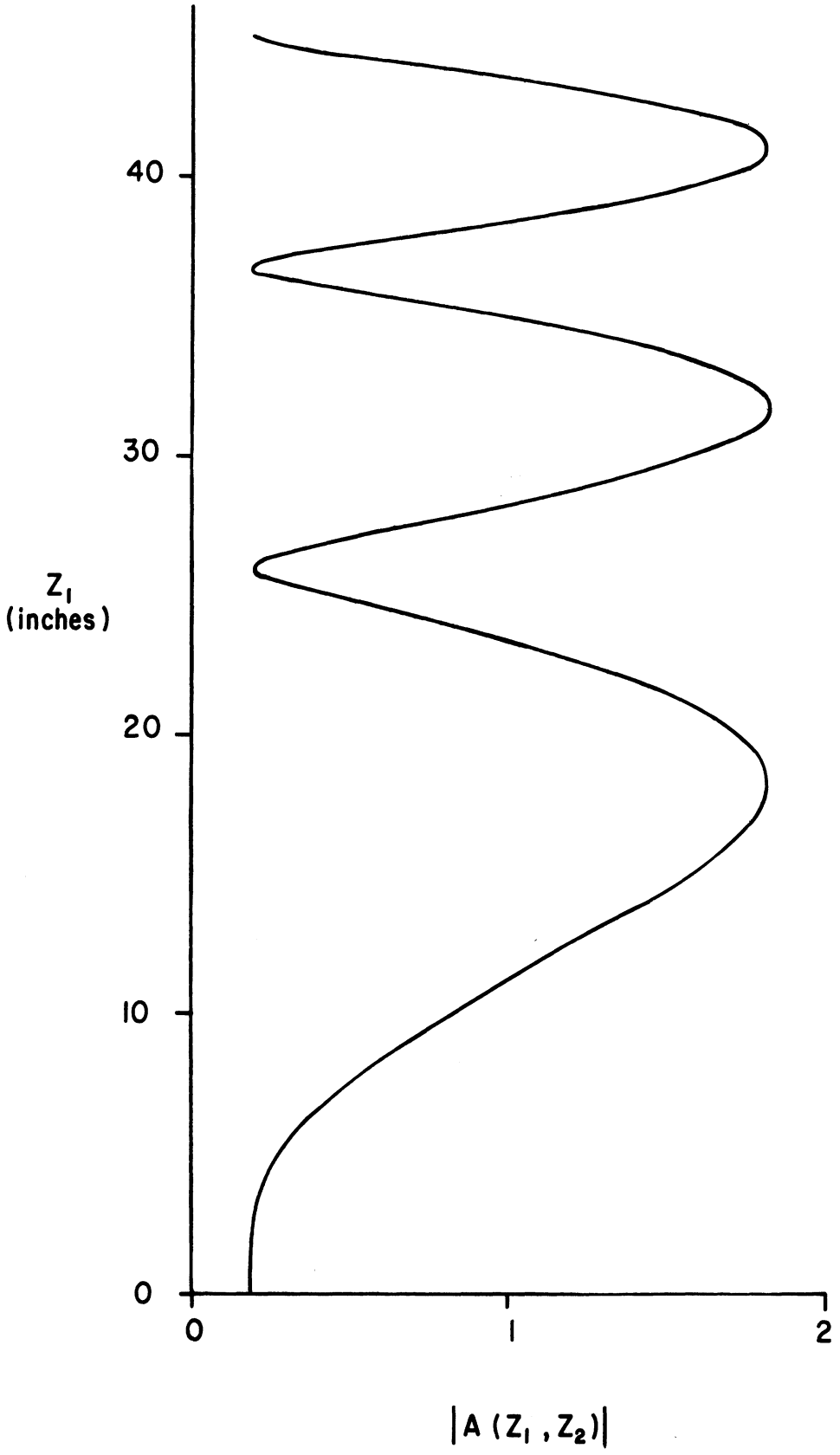

Fig. 6: Amplitude variation of received voltage when $z_2 = z_1$.

that $z_1 = 41.01$ inches is indeed the third maximum above the earth. Reducing the common height to 36.68 inches produces 45 dB reduction in the signal. For z_1 held fixed at 41 and 39 inches, the variations as a function of receiver height are shown in Fig. 7.

When the system is perturbed by the introduction of a scattering body, the scatterer must also be imaged in the ground, but since the image is a localized one only when the ground is perfectly conducting and its use is an approximation under all other circumstances, the strength that must be assigned to the image scatterer is not immediately apparent. However, only one choice is logical, and this is evident from Fig. 8. When the ground is "removed" in favor of an image transmitter T' and an image scatterer S', four scattered signals are received corresponding to the scattering of the fields radiated by the actual and image transmitters by the body and its image. According to ray theory, the ray paths are as shown in Fig. 8a, and this situation must be entirely equivalent to the one shown in Fig. 8b in which rays are reflected at the ground rather than attributed to an image. The following equivalence then results:

Fig. 8a	Fig. 8b
TSR	TSR
TP_1SR	T'SR
TSP_2R	T'S'R
TP_1SP_2R	TS'R

Since any ray reflection at the ground introduces a reflection coefficient ρ, we observe that the relative strengths of the four contributions are 1, ρ, ρ and ρ^2; and if the image transmitter is assigned a strength ρ (as required by the first two lines of the Table), the image scatterer must have a strength unity when excited by the image transmitter, but a strength ρ^2 when illuminated by the actual source. We remark that these assignments are in accordance with exact theory when the ground is perfectly conducting, implying $\rho = \pm 1$.

The problem has now been reduced to that of a scatterer in free space illuminated by a single point source or dipole field. Given a solution of adequate generality, each of the four scattered field contributions at the receiving antenna can be obtained

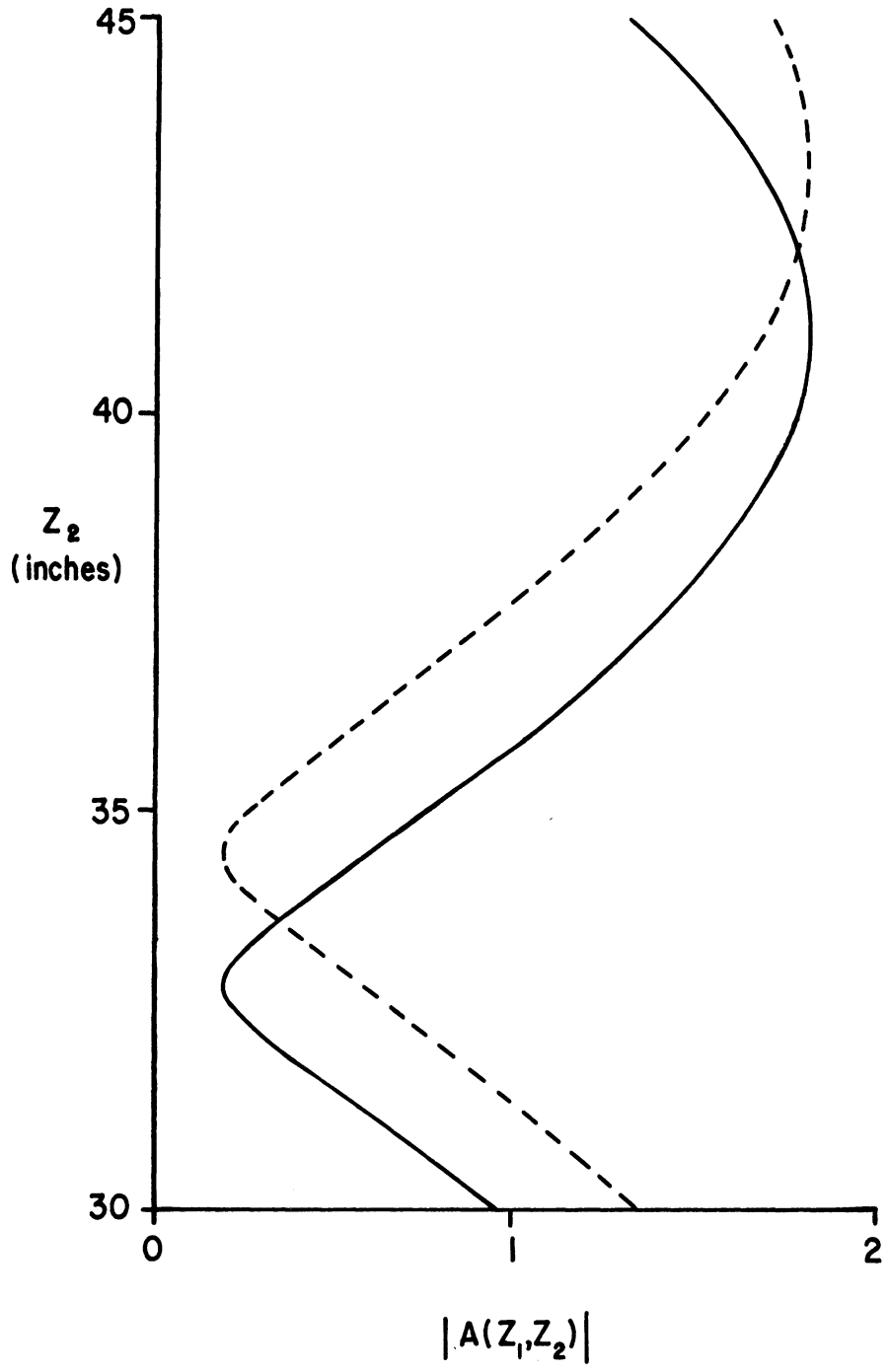

Fig. 7: Amplitude variation of the received voltage as a function of receiver height for z_1 = 41 inches (—) and z_1 = 39 inches (---).

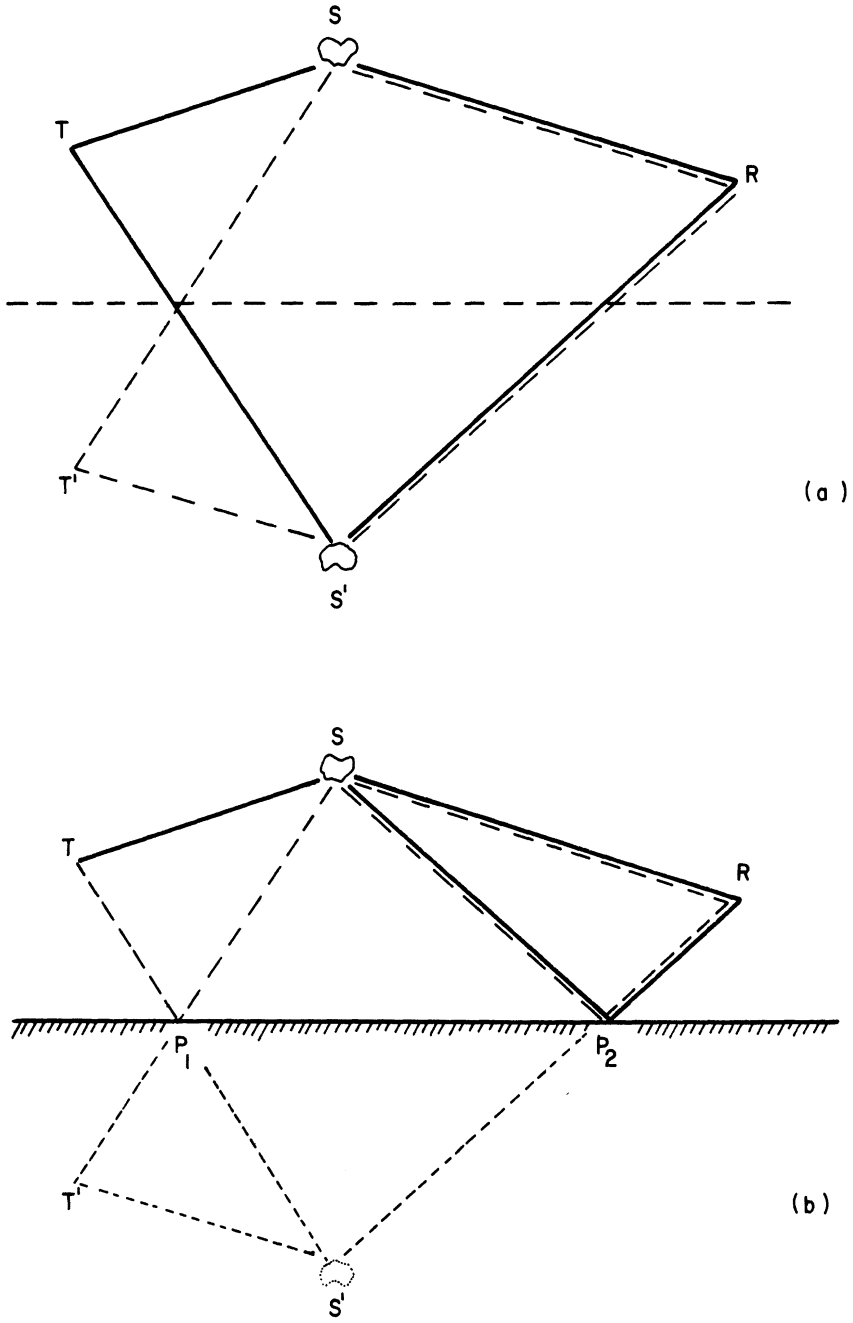

Fig. 8: Equivalent ray paths.

by appropriate scaling and identification of coordinates, and an expression for the received voltage then follows immediately. The consideration of this basic scattering problem is our next task.

2. The Theoretical Model

2.1 Man as a Scatterer

In all respects, not least the way in which he scatters electromagnetic waves, man is a very complex object indeed. Were we to attempt to simulate any man precisely, the model would inevitably depend on the physique, posture, attitude, clothes, etc. of the man selected, and because of these dependences, the model may have very little relevance to the genus "homo sapiens" even if it could be found. A more profitable approach is to seek the simplest possible models which reproduce those features of the scattering important for the task in hand, and then select the specific model which most naturally "resembles" a man. It is this that we shall do.

Measurements of the radar scattering properties of a man have shown (Schultz, et al., 1958) that at X-band frequencies the backscattering cross section ranges from 1.2 to 0.7 m^2 dependent on the angle of look, and averages 0.94 m^2 independent of polarization. Were we to model a man by a dielectric cylinder of radius a and length 2b, the high frequency cross section would be

$$\sigma = 4|\rho|^2 kab^2 \qquad (11)$$

where ρ is the Fresnel reflection coefficient for normal incidence: see Eq. (2) with $\theta = 90^o$. Judged by the volume and cross sectional (or shadow) area of a typical man, we are led to choose a = 0.5 ft, b = 3 ft, and to fit the measured data we would then require that $\epsilon = 1.48$. The fact that this is much less than the average permittivity of the biological materials themselves is because a man does not have the specular scattering capability of the smooth surface of our model.

As the bistatic scattering angle increases to 90^o, the measured radar cross section of a man decreases by about 25 percent and then rises slowly, but remains independent of the polarization. To simulate this behavior it would be necessary to change the radius and/or permittivity of the cylinder, and to do so differently for the two principal polarizations. Fortunately we are spared this task. Our concern is

with angles fairly close to forward, and though no measured data have been found for angles greater than 90^{o}, the near forward scattering from any body is primarily determined by its shadow forming capability. Provided the body is opaque, its material properties are relatively unimportant, and this allows us to select any body whose geometric shadow is comparable to that cast by a man. Our initial choice is a perfectly conducting right circular cylinder.

2.2 Plane Wave Scattering by a Cylinder

We consider first the simple case in which the cylinder is illuminated by a plane wave incident in a plane perpendicular to the z axis of the cylinder, with its electric vector in this plane. The task is to obtain an expression for the scattered field in a direction close to forward, and at large distances from the cylinder but not necessarily in the far zone.

Since the body is perfectly conducting, the scattered field is determined by the electric Hertz vector

$$\underline{\pi}(\underline{r}) = \frac{iZ}{4\pi k} \iint_S \hat{n} \wedge \underline{H}(\underline{r}') \frac{e^{ik|\underline{r}-\underline{r}'|}}{|\underline{r}-\underline{r}'|} \, dS' \tag{12}$$

where $\underline{r}$ and $\underline{r}'$ are the position vectors of the point of observation and the variable point of integration on the surface S of the cylinder; and in terms of $\underline{\pi}$,

$$\underline{E}^{s}(\underline{r}) = \nabla \wedge \nabla \wedge \underline{\pi} \sim -k^2 \hat{r} \wedge (\hat{r} \wedge \underline{\pi}) \tag{13}$$

at large distances from the cylinder. Although the exact surface field is unknown, physical optics should constitute a reasonable approximation because of the large electrical dimensions of the cylinder. According to this approximation, the surface field is

$$\hat{n} \wedge \underline{H} = \begin{cases} 2\hat{n} \wedge \underline{H}^{i} & \text{on the illuminated portion} \\ 0 & \text{on the shadowed portion} \end{cases}$$

where the affix "i" denotes the incident field. Equation (12) then becomes

$$\underline{\pi}(\underline{r}) = \frac{iZ}{2\pi k} \iint \hat{n} \wedge \underline{H}^i(\underline{r}') \frac{e^{ik|\underline{r}-\underline{r}'|}}{|\underline{r}-\underline{r}'|} dS' \tag{14}$$

where the integration is confined to the "front" half of the curved surface of the cylinder, and for a given incident field, this is an explicit integral which can be evaluated.

We choose

$$\underline{E}^i = \hat{y} e^{ikx}, \qquad \underline{H}^i = Y \hat{z} e^{ikx} \tag{15}$$

representing a plane wave propagating in the positive x direction with its electric vector perpendicular to the axis of the cylinder, and take the point of observation to be in the plane $z = 0$ displaced a distance Δ from the perpendicular bisector of the cylinder. If ρ and ϕ are cylindrical coordinates such that $x = \rho \cos\phi$, $y = \rho \sin\phi$, the curved surface of the cylinder is $\rho = a$ and the illuminated portion is (see Fig. 9)

$$\pi/2 \leq \phi' \leq 3\pi/2, \qquad -b+\Delta \leq z' \leq b+\Delta .$$

Since

$$\underline{r} = r(\hat{x}\cos\phi + \hat{y}\sin\phi) = r\hat{r}$$

$$\underline{r}' = a(\hat{x}\cos\phi' + \hat{y}\sin\phi') + z'\hat{z}$$

and

$$\hat{n} = \hat{x}\cos\phi' + \hat{y}\sin\phi' ,$$

it is a trivial matter to express (14) as a double integral over ϕ' and z', and when this is substituted into (13) we have

$$\underline{E}^s(\underline{r}) \sim (-\hat{x}\sin\phi + \hat{y}\cos\phi) \frac{e^{ikr}}{kr} S(\phi) \tag{16}$$

where

$$S(\phi) = -\frac{ik^2 a}{2\pi} \int_{-b+\Delta}^{b+\Delta} \int_{\pi/2}^{3\pi/2} \cos(\phi' - \phi) e^{ika\cos\phi'} \frac{r}{|\underline{r}-\underline{r}'|} e^{ik(|\underline{r}-\underline{r}'| - r)} d\phi' dz' . \tag{17}$$

We note that the forward scattering direction is $\phi = 0$.

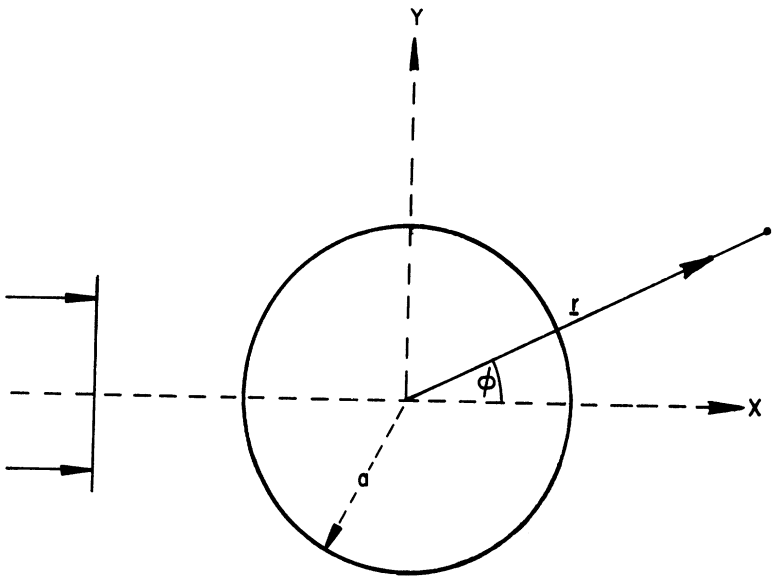

z axis out of paper

Fig. 9: Geometry for the cylindrical scattering problem.

In the amplitude factors of the integrand, r' can be neglected in comparison with r, but the phase factor needs more careful attention. Provided $r > \max r'$,

$$|\underline{r} - \underline{r}'| = r - \hat{r}\cdot\underline{r}' + \frac{1}{2r}\left\{r'^2 - (\hat{r}\cdot\underline{r}')^2\right\} + \frac{1}{2r^2}(\hat{r}\cdot\underline{r}')\left\{r'^2 - (\hat{r}\cdot\underline{r}')^2\right\} + O(r^{-3}) \qquad (18)$$

giving

$$k\left\{|\underline{r} - \underline{r}'| - r\right\} = -ka\cos(\phi' - \phi) + \frac{k}{2r}\left\{a^2\sin^2(\phi' - \phi) + z'^2\right\}$$

$$+ \frac{ka}{2r^2}\cos(\phi' - \phi)\left\{a^2\sin^2(\phi' - \phi) + z'^2\right\} + O(r^{-3}). \qquad (19)$$

The standard far field situation is that in which the second and all subsequent terms on the right hand side of (19) can be neglected. If the criterion for neglecting a term is that its contribution to the phase shall not exceed $\pi/8$, that portion of the second term which depends on ϕ' is negligible if

$$r \geq \frac{2}{\lambda}(2a)^2$$

requiring $r \geq 21.4$ ft if $a = 0.5$ ft .

Because of the nature of the ϕ' factor, this is actually an over estimate of the range required, and in any case the criterion is adequately fulfilled at all ranges of interest to us to justify omitting this portion of the second (and all subsequent) terms in (19). However, the terms involving z' are another matter. Even when the offset distance $\Delta = 0$, the choice $b = 3$ ft implies that the second term on the right hand side of (19) must be retained unless $r \geq 770.4$ ft, and to retain the second but omit the third term demands $r \geq 19.6$ ft.

With the retention of the second order (quadratic) phase terms in z', the ϕ' and z' integrals separate and the expression for $S(\phi)$ becomes

$$S(\phi) = \frac{ik^2ab}{\pi} I \int_{-\pi/2}^{\pi/2} \cos(\phi' - \phi)\exp\left\{2ika\sin\frac{\phi}{2}\sin(\phi' - \frac{\phi}{2})\right\}d\phi' \qquad (20)$$

with

$$I = \frac{1}{2b} \int_{-b+\Delta}^{b+\Delta} \exp\left\{ i \frac{k}{2r} z'^2 \right\} dz' \quad . \tag{21}$$

If $2ka \sin \frac{\phi}{2} >> 1$, the ϕ' integral can be asymptotically evaluated using the stationary phase method to yield the geometrical optics expression for the scattered field, but this is no longer valid in directions close to forward where $2ka \sin \frac{\phi}{2} \lesssim 1$. An alternative approach which is effective in this region is to use the identity

$$\cos(\phi' - \phi) = \cos(\phi' - \tfrac{\phi}{2}) \cos \tfrac{\phi}{2} + \sin(\phi' - \tfrac{\phi}{2}) \sin \tfrac{\phi}{2} \quad ,$$

in which case

$$S(\phi) = \frac{ik^2 ab}{\pi} I(r) \left\{ \cos^2 \frac{\phi}{2} \operatorname{sinc}(ka \sin \phi) + B(\phi) \right\} \tag{22}$$

where

$$\operatorname{sinc} X = \frac{\sin X}{X}$$

and

$$B(\phi) = \frac{1}{2} \sin \frac{\phi}{2} \int_{-\pi/2}^{\pi/2} \sin(\phi' - \tfrac{\phi}{2}) \exp\left\{ 2ika \sin \tfrac{\phi}{2} \sin(\phi' - \tfrac{\phi}{2}) \right\} d\phi' \quad .$$

Clearly $B(0) = 0$ and for $2ka \sin \frac{\phi}{2} << 1$, $B(\phi) \simeq - \sin^2 \frac{\phi}{2}$. Unfortunately, we will be concerned with values of ϕ as large as 20°, implying $2ka \sin \frac{\phi}{2}$ as large as 12, and since $B(\phi)$ provides the dominant contribution to the scattering from a metallic cylinder at wide angles, there is no way to justify omitting $B(\phi)$ from the scattering problem.

On the other hand, the metallic cylinder is a reasonable model of a man only in directions close to forward and there are good reasons, both theoretical and practical, for retaining only the sinc term in (22). Physical optics is only an approximate method and overestimates the magnitude of $B(\phi)$ for small ϕ. An exact

analysis for a circular cylinder shows that the correction to the sinc term is attributable to creeping waves, and even for a metallic cylinder

$$|B| \sim \frac{1}{2}\sqrt{\pi}\,(ka/2)^{-2/3}\,q$$

(Bowman, et al., 1969; p. 112) where q is of order 0.3 throughout the angular range of interest. Since it is unlikely that the irregular surface of a man could actually support creeping waves, it is logical to suppress their contribution in our simulation, in which case

$$S(\phi) = \frac{ik^2 ab}{\pi}\, I(r)\, \mathrm{sinc}(ka \sin\phi) \tag{23}$$

where we have assumed $\cos^2 \frac{\phi}{2}$ can be replaced by unity. Comparison with Eq. (4.194) of Bowman, et al. (1969) shows that (23) is identical to the scattering amplitude for a perfectly conducting rectangular plate whose dimensions are those of the shadow cast by the cylinder. In effect, the approximations which have been applied to Eq. (22) have reduced the cylindrical model to the simpler planar one, and this was actually the model used by Row and Abraham (1965) in their investigation of anti-intrusion systems. As we shall see, the simulation is adequate provided the range effect represented by the function I is retained.

2.3 Plane Wave Scattering by a Rectangular Plate

To set the stage for the analysis which will follow, it is convenient to parallel the above derivation in the simpler case of a rectangular plate, and to examine the role played by the range factor I in relation to this geometry.

Consider, therefore, a thin perfectly conducting rectangular plate occupying the region $-a \leq y \leq a$, $-b+\Delta \leq z \leq b+\Delta$ of the plane $x = 0$. For the incident field defined in Eq. (15), the illuminated portion of the surface is the face $x = -0$ where the outward unit vector normal is $\hat{n} = -\hat{x}$. The physical optics expression for the scattered field is then given by Eq. (16) with

$$S(\phi) = \frac{ik^2}{2\pi} \cos\phi \int_{-b+\Delta}^{b+\Delta} \int_{-a}^{a} e^{ik(|\underline{r}-\underline{r}'| - r)}\, dy'dz' \quad .$$

If $x > (y'-y)^2 + z'^2$,

$$|\underline{r}-\underline{r}'| \simeq x + \frac{1}{2x}\left\{(y'-y)^2 + z'^2\right\} \quad ,$$

equivalent to the neglect of cubic and higher order terms in the phase expansion. The y' and z' integrals now separate and

$$S(\phi) = \frac{ik^2}{2\pi} \cos\phi\, e^{ikr(\cos\phi - 1)} \int_{-b+\Delta}^{b+\Delta} \exp\left(ik\frac{z'^2}{2x}\right) dz' \int_{-a+y}^{a+y} \exp\left(ik\frac{y'^2}{2x}\right) dy' \quad . \tag{24}$$

The z' integral was previously defined as $2bI$, but both integrals in (24) have exactly the same form and can be expressed in terms of the finite range (complementary) Fresnel integral

$$F(t) = \int_0^t e^{i\mu^2}\, d\mu \quad . \tag{25}$$

Clearly $F(-t) = -F(t)$

and for $t \ll 1$

$$F(t) \simeq t \ ,$$

implying $F(0) = 0$;

whereas for $t \gg 1$

$$F(t) \sim \frac{1}{2}\sqrt{\pi}\ e^{i\pi/4} \quad .$$

In terms of the functions

$$C(z) = \sqrt{2/\pi} \int_0^{\sqrt{z}} \cos \mu^2 \, d\mu$$

$$S(z) = \sqrt{2/\pi} \int_0^{\sqrt{z}} \sin \mu^2 \, d\mu$$

tabulated by Jahnke and Emde (1945, p. 35),

$$F(t) = \sqrt{\pi/2}\, \mathrm{sgn}(t) \left\{ C(t^2) + iS(t^2) \right\} \tag{26}$$

where

$$\mathrm{sgn}(t) = \begin{cases} -1 & t < 0 \\ 1 & t > 0 \end{cases} .$$

Equation (24) can now be written as

$$S(\phi) = \frac{i2k^2 ab}{\pi} \cos \phi \, e^{ikr(\cos \phi - 1)} \, II' \tag{27}$$

where

$$I = \frac{1}{2b} \sqrt{\frac{2x}{k}} \left[F\left\{ \sqrt{\frac{k}{2x}} (b + \Delta) \right\} + F\left\{ \sqrt{\frac{k}{2x}} (b - \Delta) \right\} \right] \tag{28}$$

(see Eq. 21) and I' differs from I only in having b and Δ replaced by a and y respectively. In the particular case $\Delta = 0$,

$$I = \frac{1}{\sqrt{\tau}} F\left\{ \sqrt{\tau} \right\}$$

and is a function of the single variable $\tau = kb^2/2x$. The modulus and phase of the range function I have been computed as functions of τ, $0 \leq \tau \leq 20$, and the results are plotted in Figs. 10 and 11. For large τ, i.e., at small ranges, the phase oscillates about the mean level of 45°, but as τ decreases below 3, the phase decreases

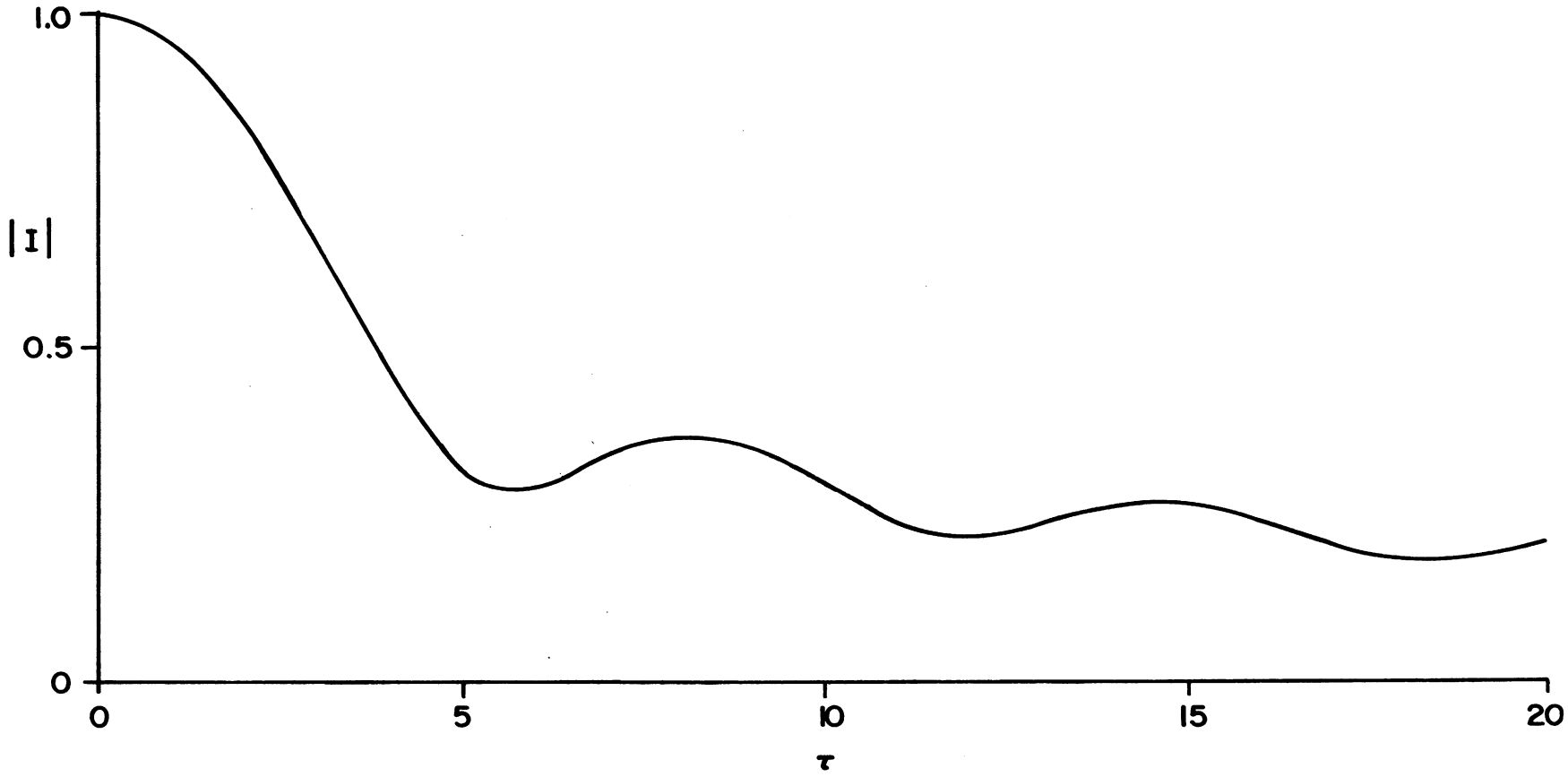

Fig. 10: Modulus of the range function I.

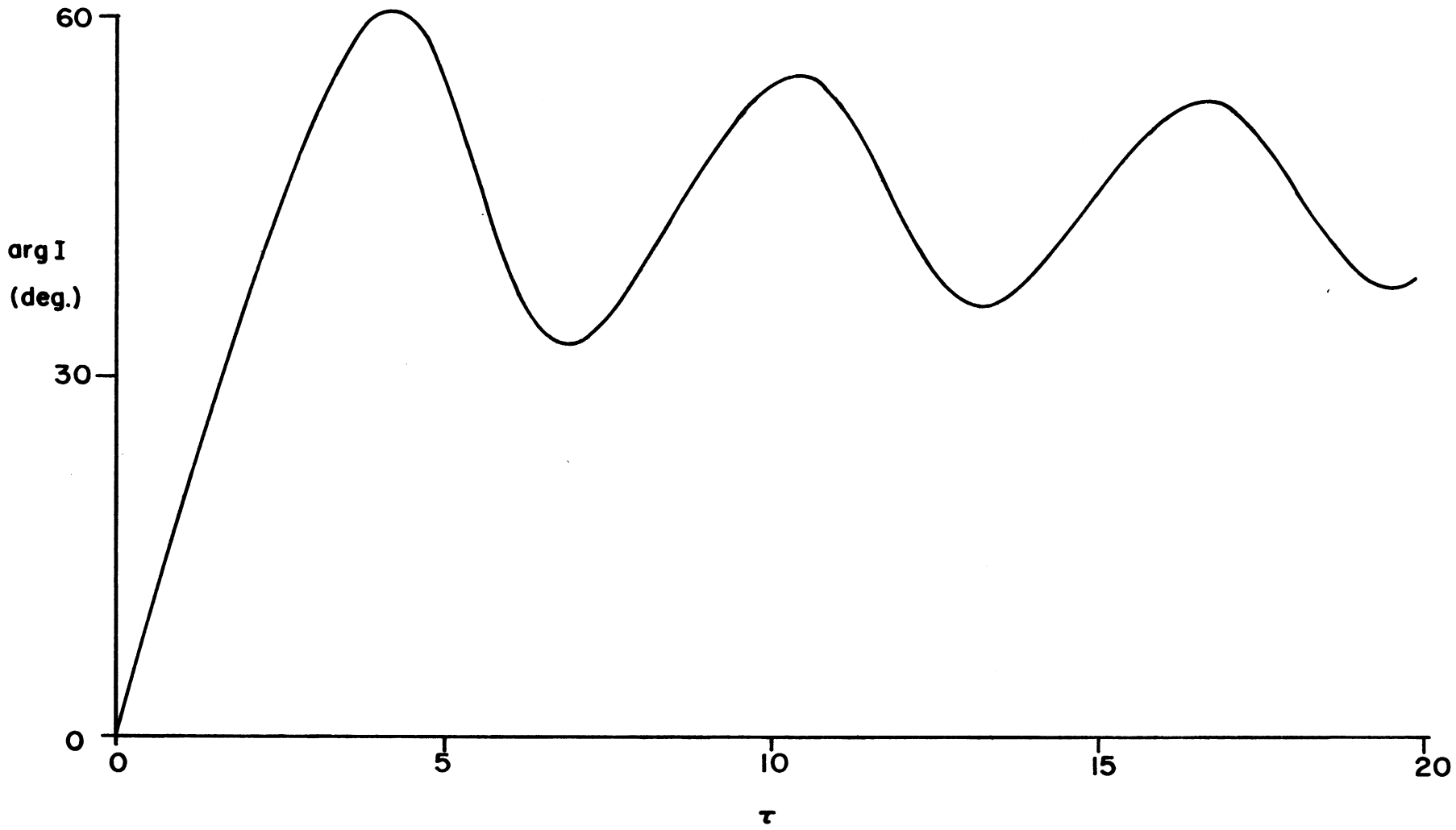

Fig. 11: Phase of the range function I.

almost linearly to zero and the modulus increases to unity. The far field is that region for which I can be replaced by unity, e.g., $\tau \lesssim 0.4$.

If x exceeds kb^2 but does not necessarily exceed $k(b \pm \Delta)^2$, I has an alternative expression which is convenient and suggestive. From the integral representation (21),

$$I = \frac{1}{2b} \int_{-b}^{b} \exp\left\{ i \frac{k}{2x} (z'^2 + 2z'\Delta + \Delta^2) \right\} dz'$$

and if $kb^2/2x \leq \pi/8$ so that the term in z'^2 can be omitted from the exponent,

$$I \simeq \frac{1}{2b} \exp(ik\Delta^2/2x) \int_{-b}^{b} \exp(ik\Delta z'/x)\, dz'$$

$$= \exp(ik\Delta^2/2x)\, \mathrm{sinc}(kb\Delta/x) \quad . \tag{29}$$

When this analysis is applied to I' and we use the fact that $r \simeq x + y^2/(2x)$ Eq. (21) is recovered precisely, showing that the expression for $S(\phi)$ in terms of the sinc function is merely a special case of the more general result (27). Nevertheless, this special case is of much interest in modelling the effect of an erect man and a rather detailed study of this formula has shown it capable of reproducing the type of perturbations that are measured. With the confidence gained from this investigation, we now proceed immediately to the general situation where the plate is offset in two directions with respect to transmitting and receiving antennas both of which are directive and at finite distances.

2.4 Simulation in the Absence of the Ground

We choose Cartesian coordinates (x, y, z) as shown in Fig. 12 with $z = 0$ defining the horizontal and, later, the level surface of the ground. The plane $y = 0$ is the boresight plane containing the transmitting and receiving antennas, and propagation is in the direction of increasing x.

A transmitting antenna at the point $\underline{r}_1 = (0, 0, z_1)$ radiates a horizontally polarized field with polar diagram $P(\alpha)$ where α is the angle measured from the

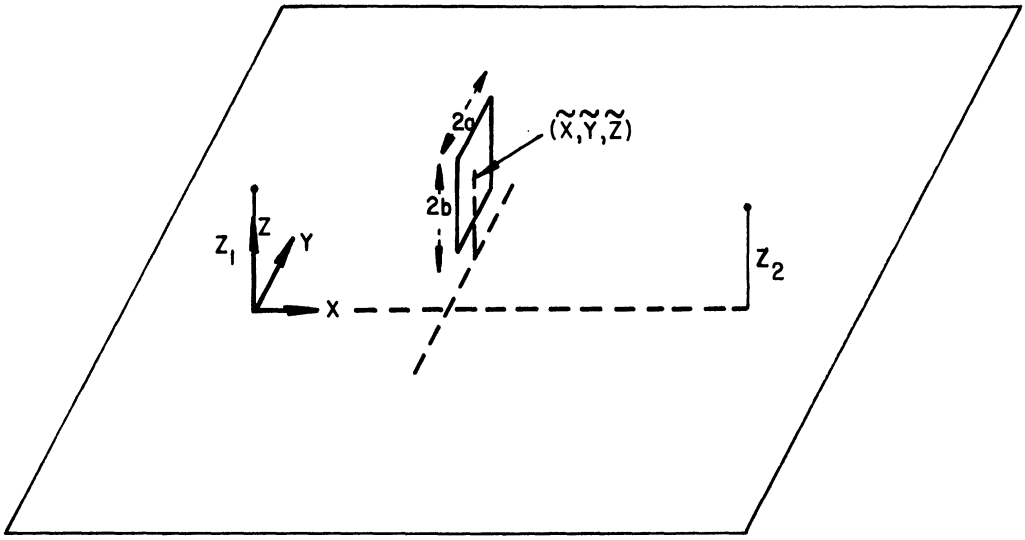

Fig. 12: Simulation geometry.

horizontal in the boresight plane, and if it is assumed that all cosine obliquity factors are absorbed into $P(\alpha)$, the unperturbed (or "incident") field at a point $\underline{r} = (x, y, z)$ in free space is

$$\underline{E}^i(x, y, z) = \hat{y}\, P(\alpha) \frac{e^{ik|\underline{r} - \underline{r}_1|}}{|\underline{r} - \underline{r}_1|} \tag{30}$$

$$\underline{H}^i(x, y, z) = Y \hat{z}\, P(\alpha) \frac{e^{ik|\underline{r} - \underline{r}_1|}}{|\underline{r} - \underline{r}_1|} \tag{31}$$

where α is, of course, a function of position. When there is no scatterer present, this is the total field at the point $\underline{r}_2 = (d, 0, z_2)$ of the receiving antenna, assumed identical to the transmitting antenna, with its polar diagram also directed horizontally, and the unperturbed (or incident) voltage is then

$$V^i = P(\alpha) P(\beta) \frac{e^{ik|\underline{r}_2 - \underline{r}_1|}}{|r_2 - r_1|} \tag{32}$$

where

$$|\underline{r}_2 - \underline{r}_1| = \left\{ d^2 + (z_2 - z_1)^2 \right\}^{1/2} \simeq d + \frac{(z_2 - z_1)^2}{2d}$$

and

$$\alpha = \beta = \tan^{-1} \frac{z_2 - z_1}{d} \quad . \tag{33}$$

We now introduce the scatterer in the form of a perfectly conducting rectangular plate of dimensions 2a by 2b occupying the region

$$\tilde{y} - a \leq y \leq \tilde{y} + a \,, \qquad \tilde{z} - b \leq z \leq \tilde{z} + b$$

of the plane $x = \tilde{x}$, where $0 < \tilde{x} < d$. The plate will perturb the field, and the added (or "scattered") contribution at an arbitrary point $\underline{r}$ is given by an electric Hertz vector whose physical optics expression is

$$\underline{\pi}(\underline{r}) = \frac{iZ}{2\pi k}\iint (-\hat{x} \wedge \underline{H}^i)\,\frac{e^{ik|\underline{r}-\underline{r}'|}}{|\underline{r}-\underline{r}'|}\,dy'dz'$$

where the integration is over the illuminated face $x = \tilde{x} - 0$ of the plate. On inserting the expansion (31), we have

$$\underline{\pi}(\underline{r}) = \frac{i}{2\pi k}\,\hat{y}\iint P(\alpha)\,\frac{e^{ik|\underline{r}'-\underline{r}_1|}}{|\underline{r}'-\underline{r}_1|}\,\frac{e^{ik|\underline{r}-\underline{r}'|}}{|\underline{r}-\underline{r}'|}\,dy'dz'$$

and since $P(\alpha)$ can be assumed to vary little over the surface of the plate, α can be assigned the value appropriate to (say) the midpoint of the plate. $P(\alpha)$ is then a constant and can be removed from the integral with

$$\alpha = \tilde{\alpha} = \tan^{-1}\frac{\left\{\tilde{y}^2 + (\tilde{z}-z_1)^2\right\}^{1/2}}{\tilde{x}}\quad , \tag{34}$$

and if $\underline{r}$ is such that the quadratic approximation

$$|\underline{r}-\underline{r}'| = \left\{(x-\tilde{x})^2 + (y-y')^2 + (z-z')^2\right\}^{1/2}$$

$$\simeq x - \tilde{x} + \frac{1}{2(x-\tilde{x})}\left\{(y-y')^2 + (z-z')^2\right\}^{1/2}$$

to the phase is adequate,

$$\underline{\pi}(\underline{r}) = \frac{i}{2\pi k}\,\hat{y}\,P(\tilde{\alpha})\frac{e^{ikx}}{\tilde{x}(x-\tilde{x})}\,\Gamma(\underline{r}) \tag{35}$$

where

$$\Gamma(\underline{r}) = \int_{\tilde{y}-a}^{\tilde{y}+a}\int_{\tilde{z}-b}^{\tilde{z}+b} \exp\left[\frac{ik}{2}\left(\frac{1}{\tilde{x}}\left\{y'^2 + (z'-z_1)^2\right\} + \frac{1}{x-\tilde{x}}\left\{(y-y')^2 + (z-z')^2\right\}\right)\right] dy'dz' \ . \tag{36}$$

At the location $\underline{r} = \underline{r}_2$ of the receiving antenna, the scattered field is

$$\underline{E}^s(\underline{r}_2) \simeq -k^2 \hat{r}_2 \wedge (\hat{r}_2 \wedge \underline{\pi})$$

and if we again absorb all cosine obliquity factors into the polar diagram $P(\beta)$ and assign β the value

$$\beta = \tilde{\beta} = \tan^{-1} \frac{\left\{\tilde{y}^2 + (z_2 - \tilde{z})^2\right\}^{1/2}}{d - \tilde{x}} \tag{37}$$

appropriate to the midpoint of the plate, the added voltage is

$$V^s = \frac{ik}{2\pi} P(\tilde{\alpha}) P(\tilde{\beta}) \frac{e^{ikd}}{\tilde{x}(d - \tilde{x})} \Gamma(\underline{r}_2) \quad . \tag{38}$$

The net voltage is therefore

$$V = V^i + V^s$$

and when this is normalized with respect to the voltage V^i in the absence of the perturbation, we obtain the result

$$\frac{V}{V^i} = 1 + \frac{ik}{2\pi} \frac{P(\tilde{\alpha})}{P(\alpha)} \frac{P(\tilde{\beta})}{P(\beta)} \exp\left\{-ik(z_2 - z_1)^2/2d\right\} \frac{d}{\tilde{x}(d - \tilde{x})} \Gamma(r_2) \quad . \tag{39}$$

The evaluation of the double integral expression (36) for $\Gamma(\underline{r}_2)$ is facilitated by introducing the quantites γ and ϵ where

$$\frac{1}{\gamma} = \frac{1}{\tilde{x}} + \frac{1}{d - \tilde{x}} \tag{40}$$

$$\epsilon = \frac{z_1}{\tilde{x}} + \frac{z_2}{d - \tilde{x}} \quad . \tag{41}$$

After some manipulation, the integrand reduces to

$$\exp\left[\frac{ik}{2\gamma}\left\{y'^2+(z'-\epsilon\gamma)^2+\frac{\gamma}{d}(z_2-z_1)^2\right\}\right]$$

and the y' and z' integrals are now of the general form shown in Eq. (14). Hence

$$\Gamma(\underline{r}_2) = \frac{2\gamma}{k}\exp\left\{ik(z_2-z_1)^2/2d\right\}\left[F\left\{\sqrt{\frac{k}{2\gamma}}(\tilde{y}+a)\right\}-F\left\{\sqrt{\frac{k}{2\gamma}}(\tilde{y}-a)\right\}\right]$$

$$\cdot\left[F\left\{\sqrt{\frac{k}{2\gamma}}(\tilde{z}-\epsilon\gamma+b)\right\}-F\left\{\sqrt{\frac{k}{2\gamma}}(\tilde{z}-\epsilon\gamma-b)\right\}\right] \quad (42)$$

where F is the Fresnel integral (25), and when this is substituted into (39) we have

$$\frac{V}{V^i} = 1+\frac{i}{\pi}\frac{P(\tilde{\alpha})}{P(\alpha)}\frac{P(\tilde{\beta})}{P(\beta)}\left[F\left\{\sqrt{\frac{k}{2\gamma}}(\tilde{y}+a)\right\}-F\left\{\sqrt{\frac{k}{2\gamma}}(\tilde{y}-a)\right\}\right]$$

$$\cdot\left[F\left\{\sqrt{\frac{k}{2\gamma}}(\tilde{z}-\epsilon\gamma+b)\right\}-F\left\{\sqrt{\frac{k}{2\gamma}}(\tilde{z}-\epsilon\gamma-b)\right\}\right]. \quad (43)$$

In the particular case $z_2 = z_1$ when the antenna heights are equal, $\epsilon\gamma = z_1$. If, in addition, $kb^2/2\gamma \lesssim \pi/8$,

$$F\left\{\sqrt{\frac{k}{2\gamma}}(\tilde{z}-\epsilon\gamma+b)\right\}-F\left\{\sqrt{\frac{k}{2\gamma}}(\tilde{z}-\epsilon\gamma-b)\right\}$$

$$\simeq 2b\sqrt{\frac{2\gamma}{k}}\exp\left\{ik(\tilde{z}-z_1)^2/2\gamma\right\}\operatorname{sinc}\left\{kb(\tilde{z}-z_1)/\gamma\right\} \quad (44)$$

and the situation is analogous to that treated in the latter part of Section 2.3. For computational purposes, however, it is more convenient to stick with the general form (43) in spite of the simplifications that are possible in special circumstances.

2.5 Simulation with the Ground Present

To complete our simulation of the effect of a man on the system, we must now introduce a ground whose surface is the plane $z = 0$. The ground is assumed

to have the reflection coefficient ρ, constant over the range of angles of concern to us, and when the transmitting antenna and the plate are both imaged in the ground, we find ourselves with two sources of radiation each illuminating two scattering objects. The strengths that must be assigned to the images were determined in Chapter 1.

When there is no perturbation present, the received voltage is attributable to the free space fields of the transmitter and its image. The expression for the voltage provided by the actual transmitter is given in Eq. (32), and if this is written as $V^i(z_1)$, the voltage due to the image is simply $\rho V^i(-z_1)$. The unperturbed voltage is therefore

$$V^i = V^i(z_1) + \rho V^i(-z_1) \tag{45}$$

where

$$V^i(z_1) = \left\{P(\alpha)\right\}^2 \frac{e^{ikR}}{R} \tag{46}$$

with

$$R = \left\{d^2 + (z_2 - z_1)^2\right\}^{1/2} \tag{47}$$

and α as defined in Eq. (33).

The introduction of the scatterer produces an added voltage consisting of four separate contributions. One of these is associated with the actual transmitter and the actual body and the expression for the corresponding voltage is given in Eqs. (38) and (42). If this is denoted by $V^s(z_1, \tilde{z})$, the analysis in Chapter 1 shows that the added voltage when the ground is present is

$$V^s = V^s(z_1, \tilde{z}) + \rho V^s(-z_1, \tilde{z}) + \rho V^s(-z_1, -\tilde{z}) + \rho^2 V^s(z_1, -\tilde{z}) \tag{48}$$

where

$$V^s(z_1, \tilde{z}) = \frac{i}{\pi} \frac{e^{ikR}}{R} P(\tilde{\alpha}) P(\tilde{\beta}) \left[F\left\{\sqrt{\frac{k}{2\gamma}}\,(y+a)\right\} - F\left\{\sqrt{\frac{k}{2\gamma}}\,(y-a)\right\}\right]$$
$$\cdot \left[F\left\{\sqrt{\frac{k}{2\gamma}}\,(z - \epsilon\gamma + b)\right\} - F\left\{\sqrt{\frac{k}{2\gamma}}\,(z - \epsilon\gamma - b)\right\}\right], \tag{49}$$

and γ, ϵ, $\tilde{\alpha}$, $\tilde{\beta}$ are as defined in Eqs. (40), (41), (33) and (37) respectively. We note that ϵ, $\tilde{\alpha}$, $\tilde{\beta}$, R and α are all functions of z_1, and that $\tilde{\alpha}$ and $\tilde{\beta}$ depend on $\tilde{z}$ as well.

The total signal normalized to that in the absence of the perturbation is now

$$\frac{V}{V^i} = 1 + \frac{V^s}{V^i} \tag{50}$$

where V^i and V^s are given in Eqs. (45) and (48).

3. Computed Data

A program has been written to compute the unperturbed and scattered voltages of Eqs. (45) and (48) respectively and thence the normalized voltage shown in Eq. (50). The program is in Fortran IV for use on the IBM 370/168 computer at The University of Michigan and a listing and specimen output are given in the Appendix.

The program reads the transmitter and receiver heights, the model half width, half height and center height, the modulus and phase (in radians) of the ground reflection coefficient, the frequency, and the initial, incremental and final values of the displacement $\tilde{y}$ of the model's center from the boresight plane as input data, and produces the unperturbed voltage FDIR, the scattered voltage FSCAT and the normalized voltage square (or power) MOD as functions of $\tilde{y}$. As part of this process, the appropriate values of the angles α and β are determined and fed into a function POLAR(A) which computes the polar diagram according to Eq. (1). Having this as a function enables the polar diagram to be changed without recompiling the entire program. The Fresnel integrals are computed according to the formula

$$F(\sqrt{x}) = \sqrt{\pi/2}\ \mathrm{sgn}(\sqrt{x})\ \{C(x) + iS(x)\}$$

using the subroutine CS(C, S, X) contained in the IBM System 360 Scientific Subroutine Package, Version II. Since the argument x of the cosine and sine integrals is the square of the Fresnel integral argument, the signum function is taken care of using a set of conditional IF statements.

In order to check the adequacy of our model, data were supplied for each of two men (subjects "A" and "B") walking or crawling (slithering?) in a direction perpendicular to the boresight plane at different distances from the transmitter. All of the data are for a range d = 100 ft and in most cases the corrected or "true" transmitter and receiver heights were 41 inches. The various curves of power versus displacement from the boresight plane show considerable variations from case to case, particularly in the fine structure, and such variations are evident even when a subject repeats a traverse in a manner as close as possible to the previous one. From the more than 20 sets of data that were provided, it would appear that at least part of the fine structure is due to the inevitable limb and body motion that accompanies a traverse, and the most regular and symmetrical curves were obtained when the subject limited his jiggling to the maximum extent possible.

We consider first the case of an erect man. Based on the blocking area of a typical man, our initial choice of the plate parameters a and b was a = 0.5 ft and b = 3 ft, and Figs. 13 and 14 show comparisons of theory* and experiment for a man walking across at distances of 50 and 30 ft respectively from the transmitter. The experimental curves are for subject A walking slowly with minimal limb movement and are the averages of the measured values for the subject approaching and leaving the boresight plane. On the whole, the agreement is rather good and though the theoretical curve for $\tilde{x} = 50$ ft has a somewhat deeper oscillation than the experimental one, particularly for $\tilde{y}$ in the 3 to 4 ft range, we remark that the averaging applied to the measured data tends to reduce the larger oscillations. Some of the raw experimental traces do reveal oscillations as large as those predicted by the model. To examine the effect of changing the half width a of the plate, Figs. 15 through 17 repeat the theoretical-experimental comparison of Fig. 13 but with a = 0.455, 0.375 and 0.25 ft respectively. The choice a = 0.455 ft does produce a slight improvement for $\tilde{y} \gtrsim 2$ ft at the expense of an increased discrepancy in the

* For all of the data presented the reflection coefficient ρ has been given the value shown in Eq. (3), and except where otherwise stated, $z_1 = z_2 = 41$ inches (= 3.417 ft), d = 100 ft and the plate has its lower edge on the ground.

vicinity of the main peak. This trend continues as a is decreased further, but because of the growing magnitude of the secondary peak, we have lost the character of the experimental curve by the time $a = 0.25$ ft, and the simulation is then good only for $\tilde{y} \lesssim 2$ ft.

All the experimental traces where the transmitter and receiver heights are such that the direct and ground-reflected signals are in phase have certain features in common. The more prominent features are a local maximum in the boresight plane, an absolute minimum for $\tilde{y} \simeq 1$ ft, followed by a main peak at $\tilde{y} \simeq 2$ ft, and all of these are reproduced by the theoretical model. To try to get a better feel for the optimum values of a and b for an erect man, we have computed the theoretical maxima and minima as functions of a, $0.25 \leq a\ (\text{ft}) \leq 0.75$, for $b = 3.0$ ft, and as functions of b, $2.5 \leq b\ (\text{ft}) \leq 3.25$ for $a = 0.5$ ft, all for $\tilde{x} = 50$ ft, and these are compared with the averages of the experimental values in Figs. 18 and 19. Unfortunately, the results are rather inconclusive, and do not provide any real grounds for choosing dimensions other than those suggested by a man's physical "blocking" area. We shall therefore continue to choose $a = 0.5$ ft and $b = 3$ ft to simulate a man walking across the range. If the man walks sideways, however, his blocking area will be greater, and it is logical to expect that a larger value of a would be appropriate. This is indeed the case, and Fig. 20 shows a comparison of experiment and theory for $a = 0.75$ ft. The experimental trace has a regular oscillation which would seem to be due to the swaying motion of the man resulting from his lock-step progression across the range. Obviously, the theory does not take this into account, and this apart, the agreement with experiment is reasonably good.

For a crawling man the experimental data were less numerous and much less complete. Results were available for only single passes at 50, 30 and 10 ft. Since the man slithered across on toes and elbows, he should therefore have presented a reasonably symmetric target, but the measured traces are rather asymmetric and, particularly for $\tilde{x} = 30$ ft, it is quite impossible to locate the midpoint corresponding to the boresight plane. This is evident from Fig. 21 where we show the experimental data for $x = 50$ and 30 ft and we also remark that no record was kept of the horizontal

scales. For all these reasons, it is almost impossible to make any realistic assessment of how well our model simulates a crawling man, but we have made some comparisons of theory and experiment. Figs. 22 through 24 are for a man crossing at mid range with a = 3.0 and b = 0.5, a = 3.0 and b = 0.25, and a = 3.3 and b = 0.5 ft respectively. The common experimental curve purports to be the average of the measured data about the boresight plane with the horizontal scale adjusted to best fit the theoretical curve. The agreement between theory and experiment is relatively good, particularly in Fig. 23 where even corresponding peaks match one another. At 30 ft, however, the theoretical and experimental curves (see Figs. 25 and 26) agree only in their average values, but because of the wide degree of uncertainty in the "average" experimental curve at this range, it would be unwise to make any judgment one way or another. There is certainly no evidence that the model is inadequate to simulate a crawling man, and it still seems sufficient to select values of a and b based on the cross sectional area he presents.

In the remaining figures we explore some of the system implications of the theory. For an erect man (a = 0.5 ft, b = 3 ft) walking across the range, the normalized power received for a range 100 ft long will depend on the antenna heights chosen. If the man is at mid range ($\tilde{x}$ = 50 ft) and the heights are such as to put the direct and ground reflected signals in phase quadrature or out of phase, the changed responses are shown in Figs. 27 and 28 respectively. In each case the solid line corresponds to the in-phase situation and is the same as that in Fig. 13. The main effect of having the two signals in phase quadrature is confined to distances of about a foot from the boresight plane, but having the signals out-of-phase substantially increases the normalized power and tends to interchange all maxima and minima in the pattern. Unfortunately, this last situation is not too practicable. The increased level is primarily due to a decrease in the signal when there is no intruder present and any slight change in, for example, the ground reflection coefficient would significantly affect the system. Results analogous to those in Figs. 27 and 28 but for $\tilde{x}$ = 30 and 20 ft are given in Figs. 29-32.

If the range is increased beyond 100 ft, we can still maintain the in-phase situation at the receiving antenna by adjusting the antenna heights accordingly. Table 1 lists the ranges for in-phase addition with equal antenna heights lying between 30 and 45 inches and by shifting from the third to the second and then to the first maximum above the ground it is seen that all ranges from 54 out to 602 ft can be covered with the exception of those from 201 to 267 ft. To illustrate the normalized power received at these longer ranges, Figs. 33 and 34 show the results for an erect man crossing at midrange when d = 300 and 500 ft respectively. The only substantial difference from the curves for 100 ft is a proportionate increase in the horizontal scale. This is true also of the curves in Figs. 35 and 36 for a crawling man at mid range.

Table 1: Ranges d for in-phase addition

$z_1 = z_2$	d (ft)		
(inches)	3rd max	2nd max	1st max
30	53.504	89.173	267.520
31	57.130	95.217	285.651
32	60.876	101.459	304.378
33	64.740	107.900	323.699
34	68.723	114.538	343.614
35	72.825	121.375	364.124
36	77.046	128.409	385.228
37	81.385	135.642	406.927
38	85.844	143.073	429.220
39	90.422	150.703	452.108
40	95.118	158.530	475.590
41	99.933	166.556	499.667
42	104.868	174.779	524.338
43	109.922	183.204	549.611
44	115.094	191.824	575.471
45	120.385	200.642	601.926

One possible way in which an intruder might seek to avoid detection is by "jumping", e.g., pole-vaulting, across the range. To see how feasible this might be, we have run a series of simulations for a 100 ft range with $z_1 = z_2 = 3.417$ ft and an erect man (a = 0.5 ft, b = 3 ft) with his midpoint $\tilde{z}$ at heights incremented in 0.5 ft steps from 3 ft (feet on the ground) to 15 ft (feet 12 ft above the ground). For each set of data the boresight, minimum and maximum values of the normalized power were determined, and these are plotted as functions of $\tilde{z}$ for crossings at 50, 30 and 20 ft in Figs. 37 through 39 respectively. The results are remarkably similar and if, for example, a 10 percent change in the received power is necessary for detection, the man could safely cross at all three distances by raising his feet 4 ft, i.e., midriff 7 ft, above the ground.

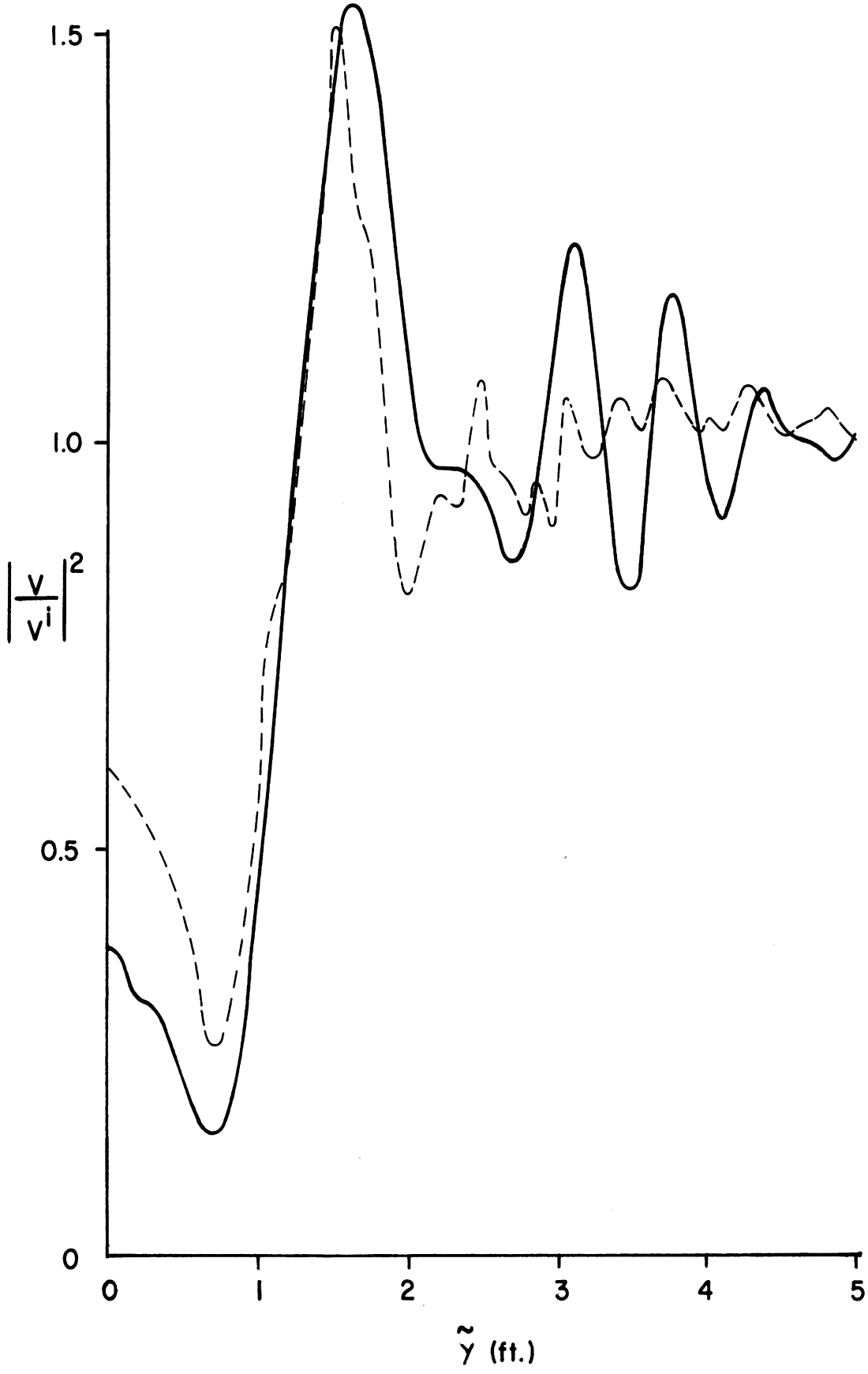

Fig. 13: Erect man at 50 ft: --- experimental (subject 'A'), —— theory for a = 0.5 ft. and b = 3 ft.

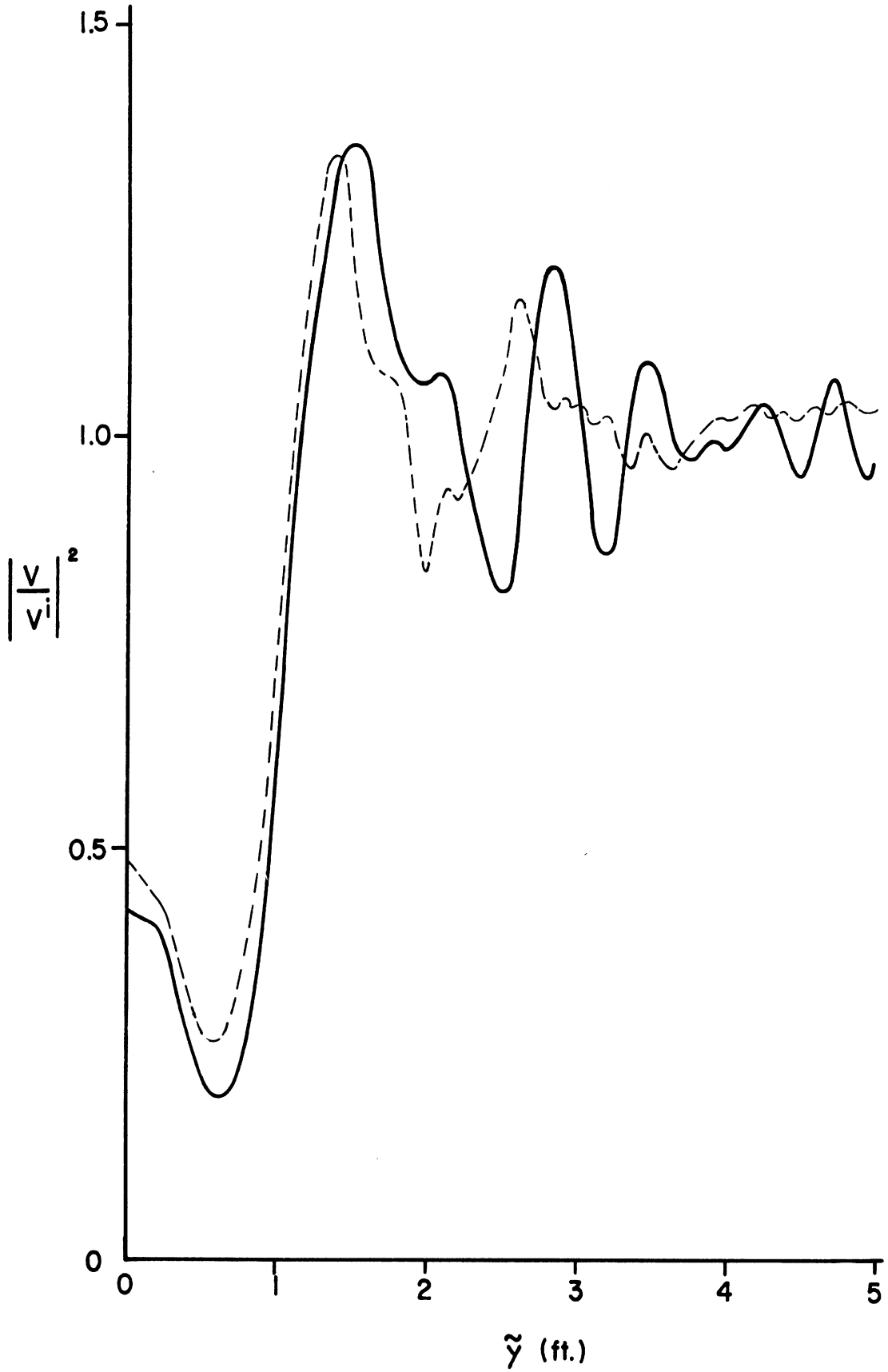

Fig. 14: Erect man at 30 ft: --- experimental (subject 'A'), —— theory for a = 0.5 ft. and b = 3 ft.

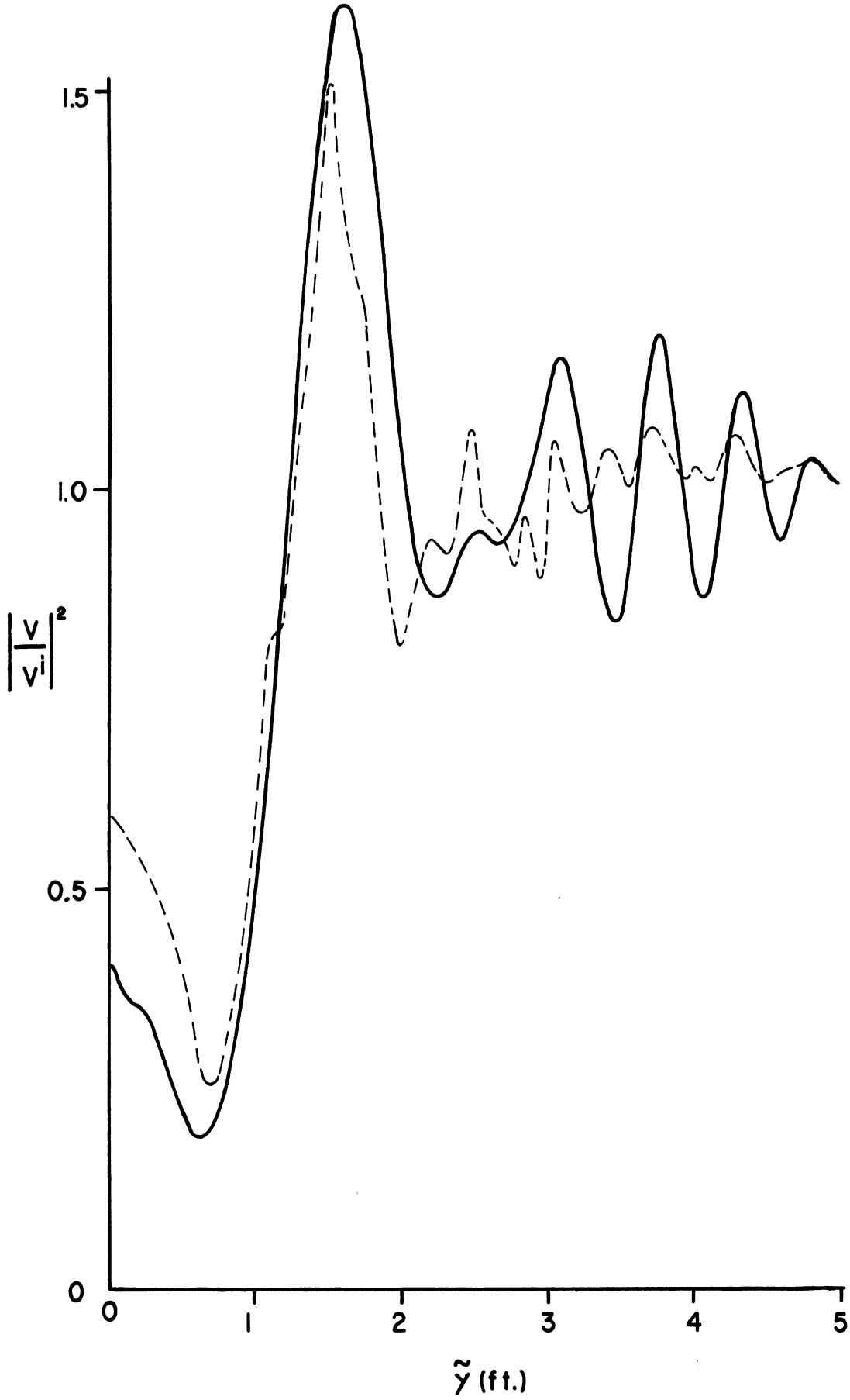

Fig. 15: Erect man at 50 ft: --- experimental (subject 'A'), —— theory for a = 0.455 ft. and b = 3 ft.

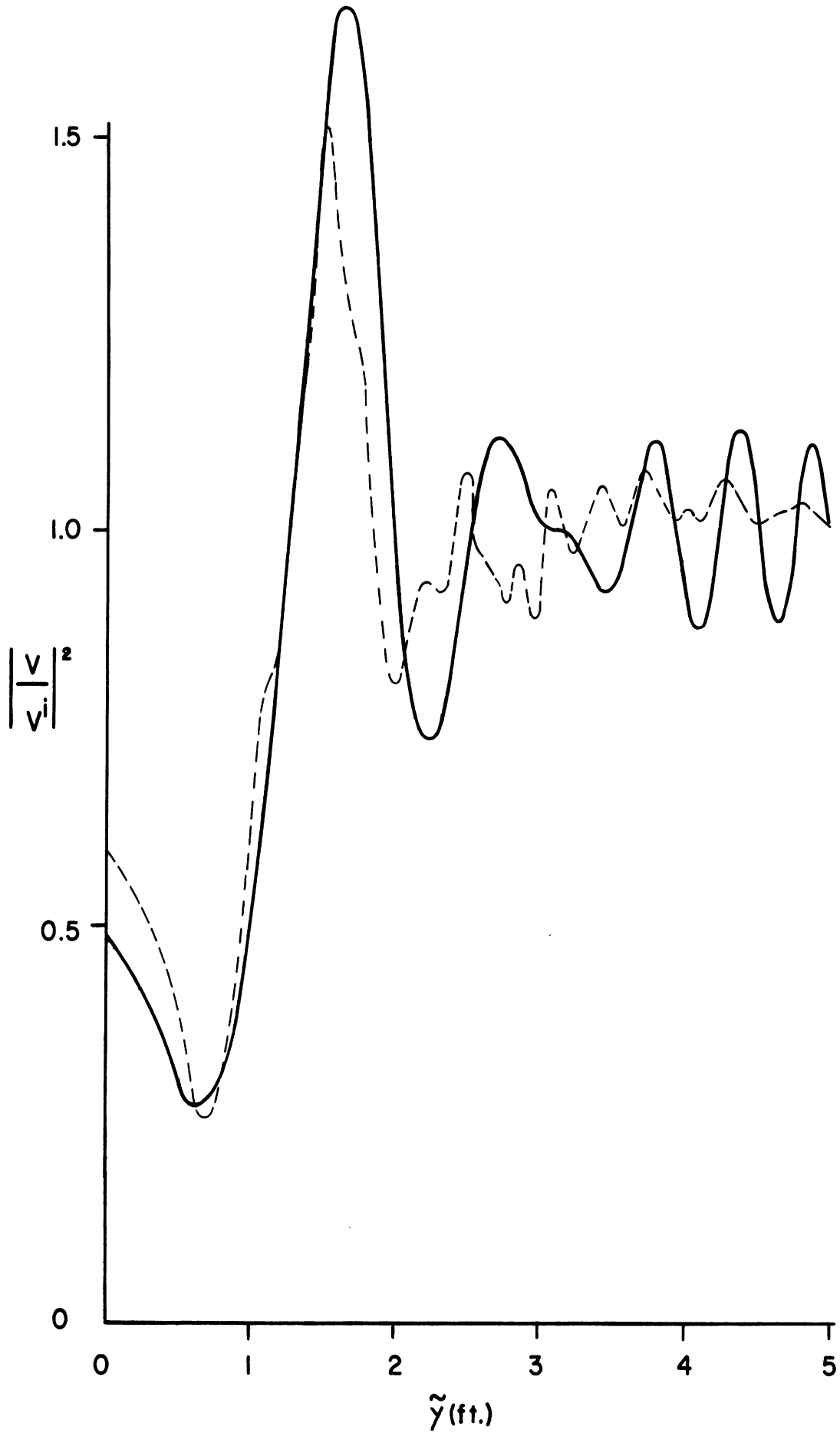

Fig. 16: Erect man at 50 ft: --- experimental (subject 'A'), —— theory for a = 0.375 ft. and b = 3 ft.

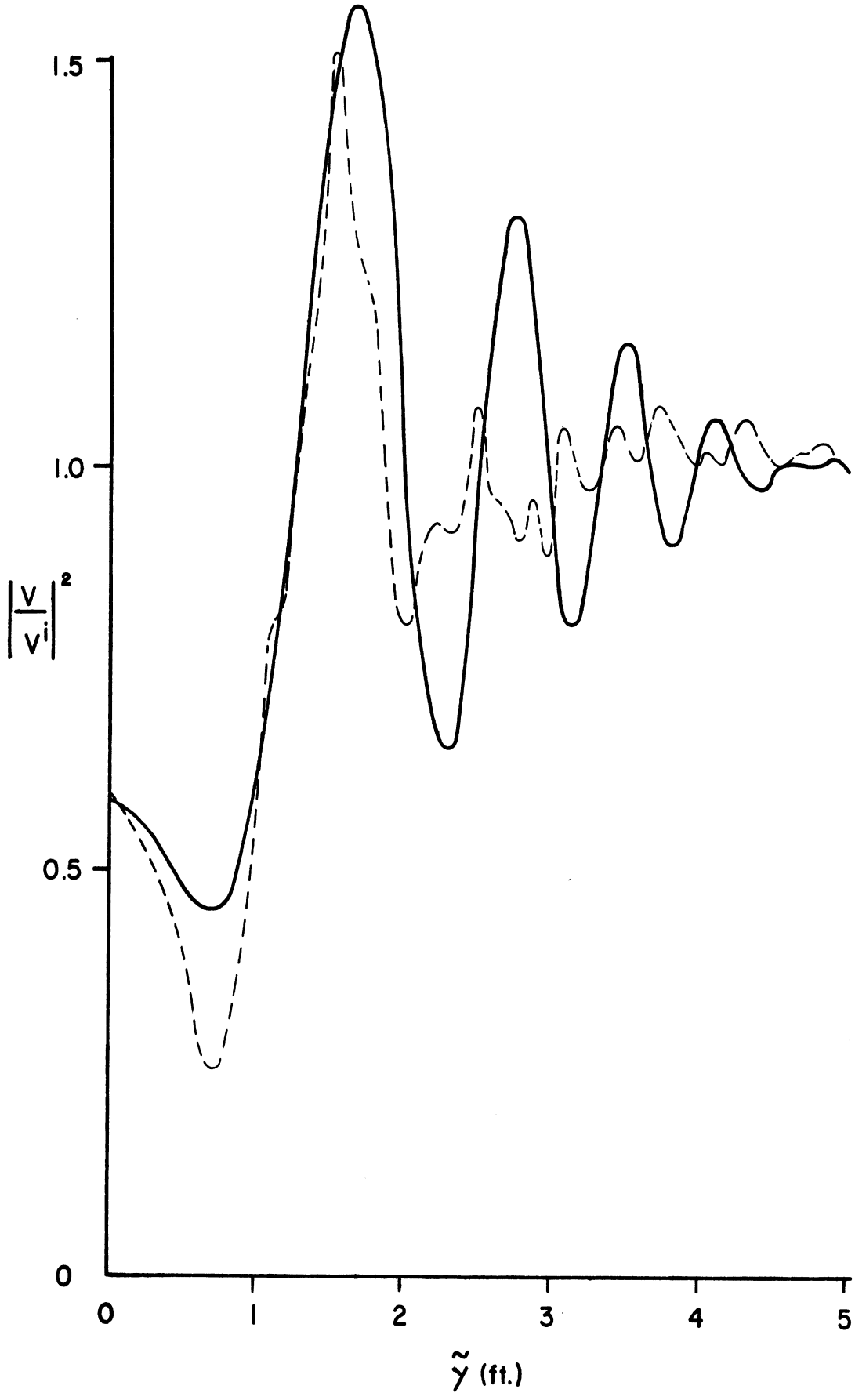

Fig. 17: Erect man at 50 ft: --- experimental (subject 'A'), —— theory for a = 0.25 ft. and b = 3 ft.

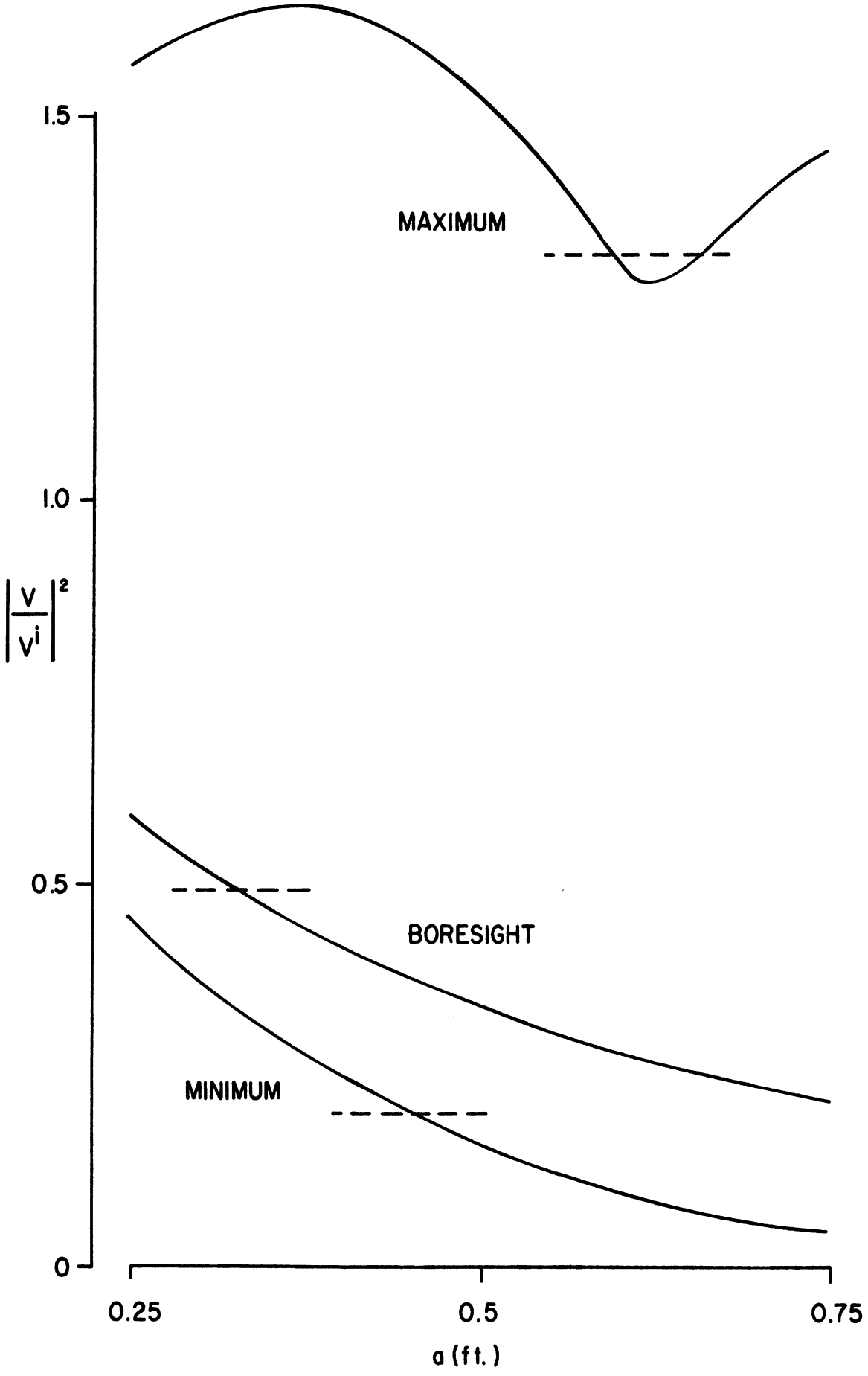

Fig. 18: Erect man at 50 ft: theoretical (——) and average experimental (---) boresight, minimum and maximum values for b = 3 ft.

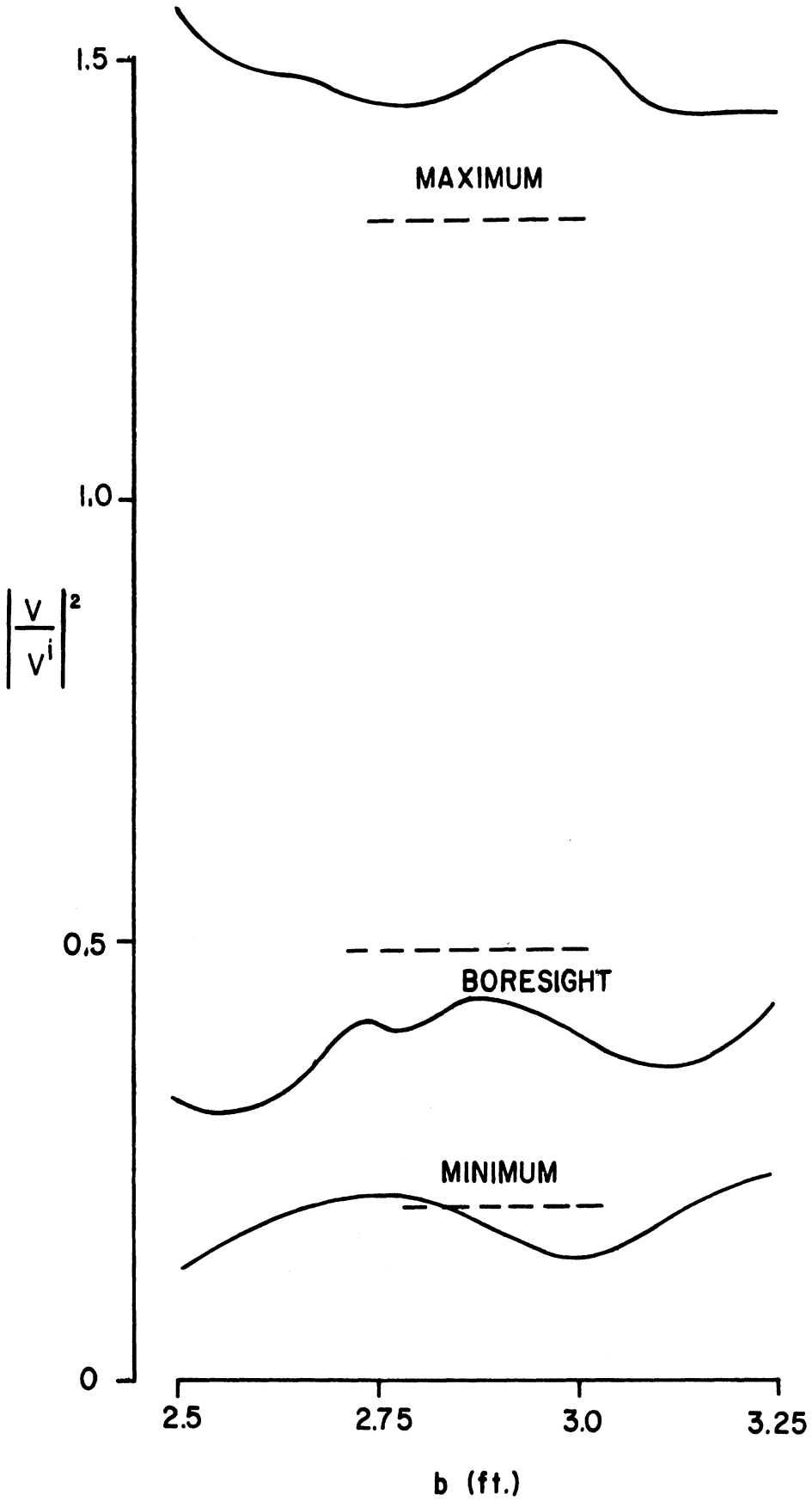

Fig. 19: Erect man at 50 ft: theoretical (——) and average experimental (---) boresight, minimum and maximum values for a = 0.5 ft.

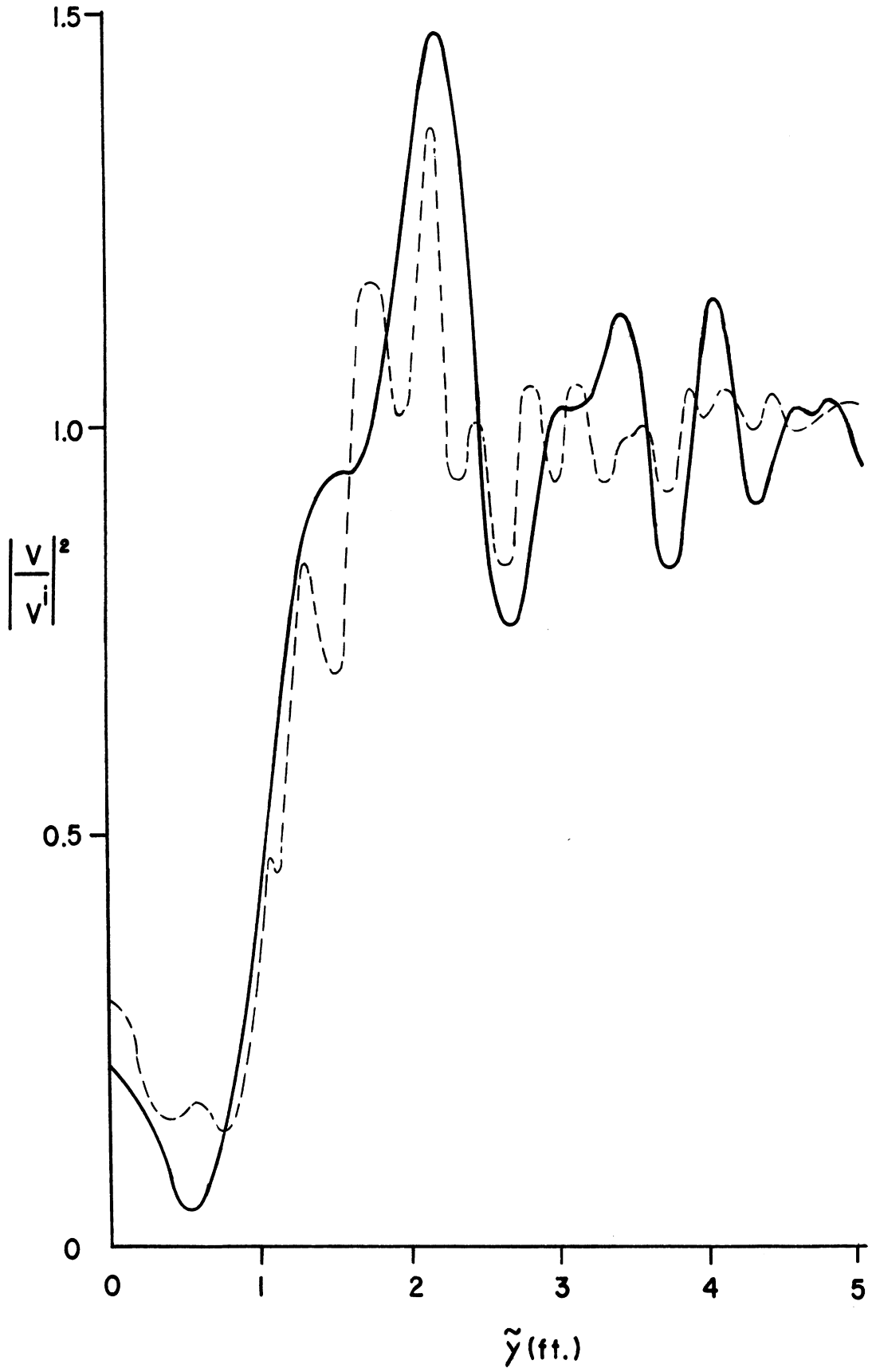

Fig. 20: Erect man moving sideways at 50 ft: --- experimental (subject 'A'), —— theory for a = 0.75 ft. and b = 3 ft.

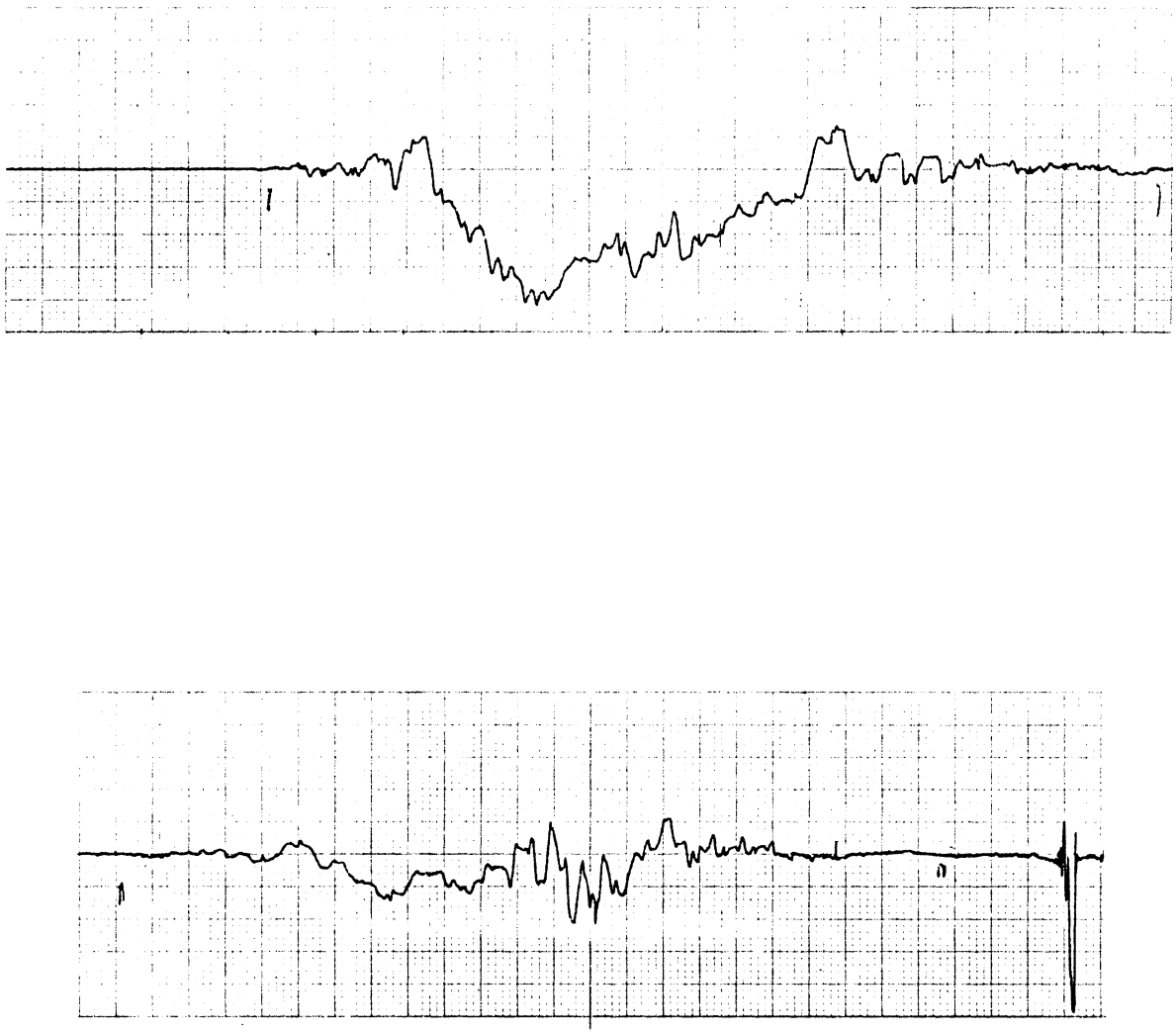

Fig. 21: Measured raw traces for a crawling man at 50 and 30 ft.

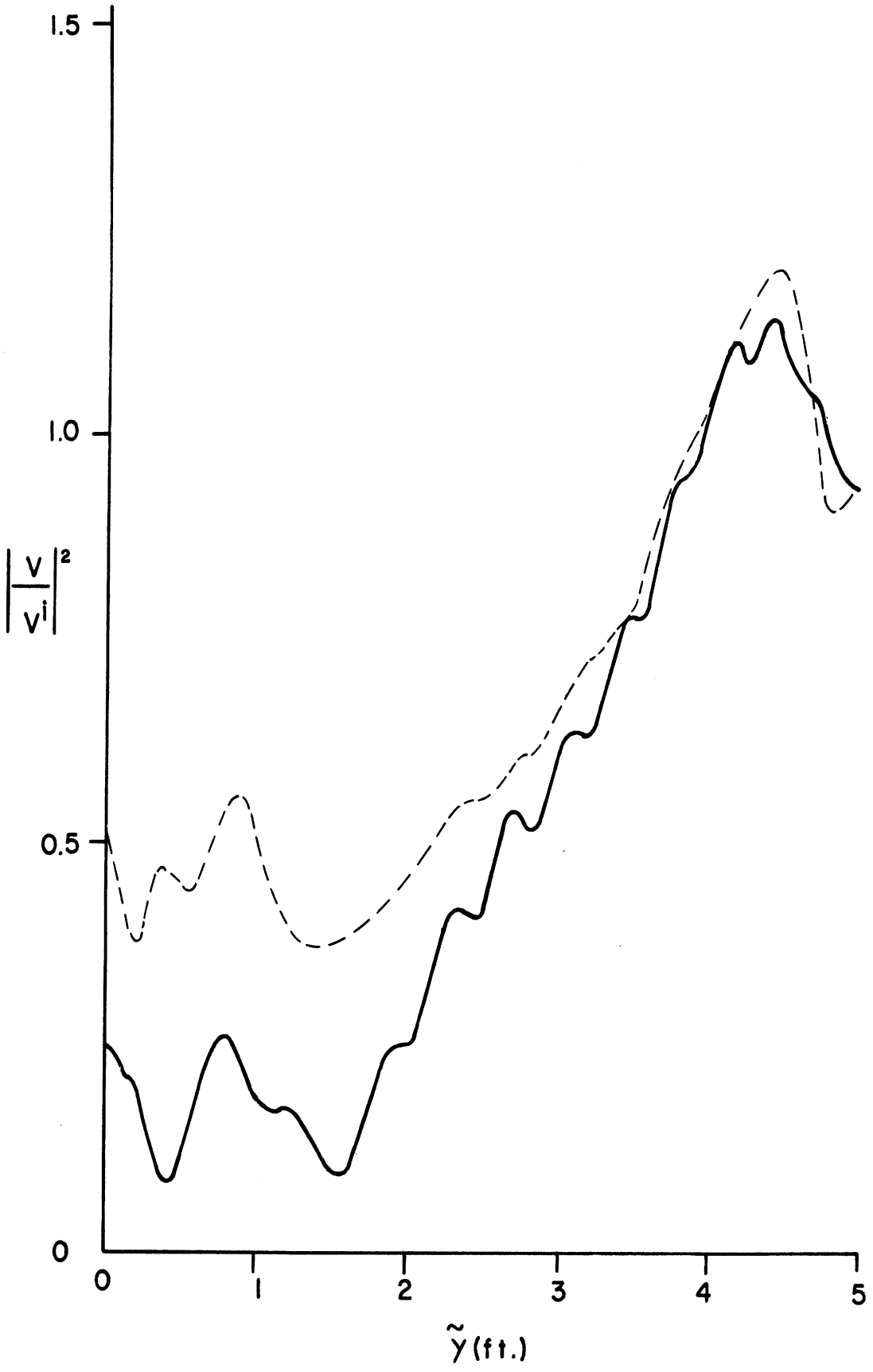

Fig. 22: Crawling man at 50 ft: --- 'average' experimental, —— theory for a = 3 ft. and b = 0.5 ft.

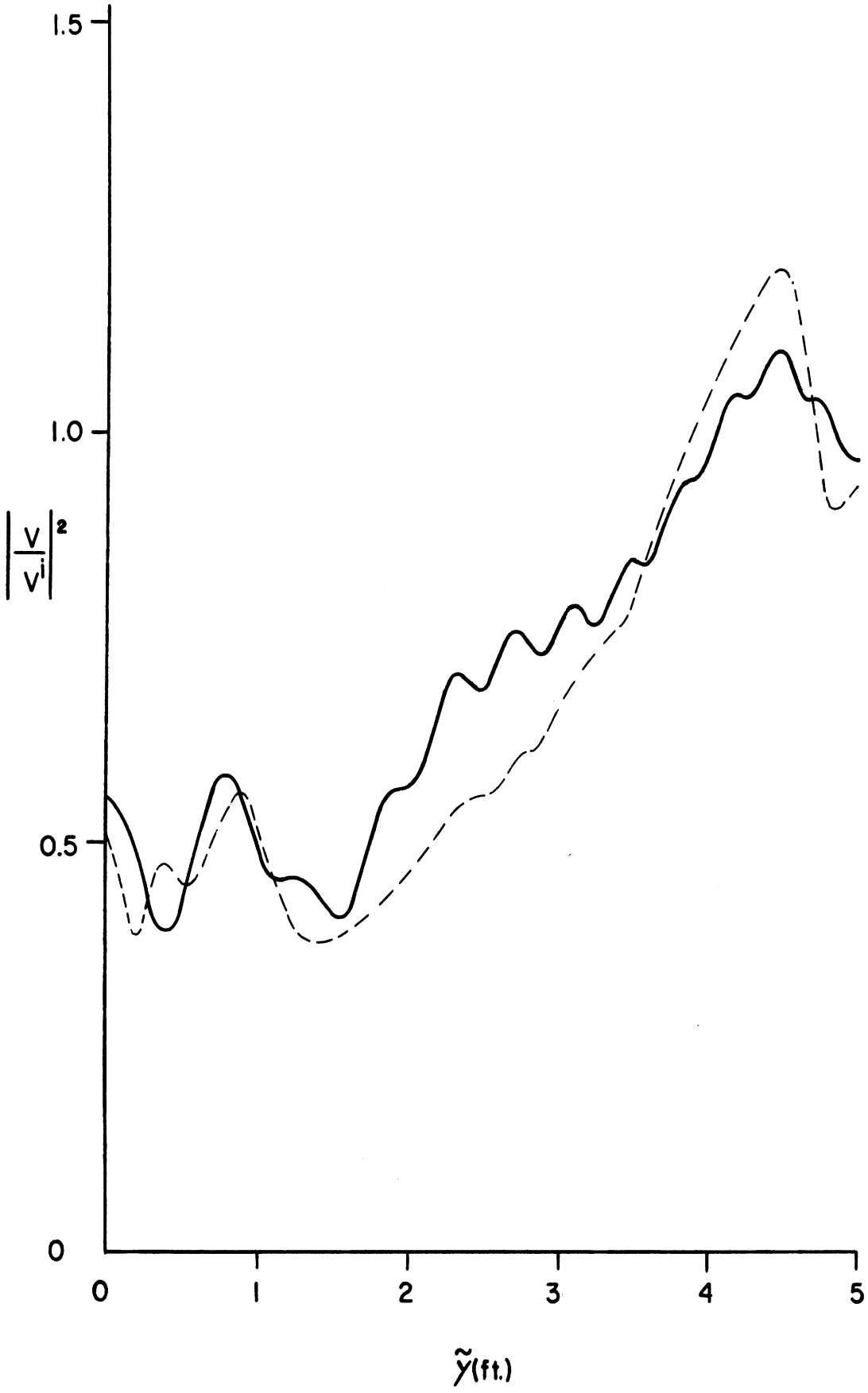

Fig. 23: Crawling man at 50 ft: --- 'average' experimental, —— theory for a = 3 ft. and b = 0.25 ft.

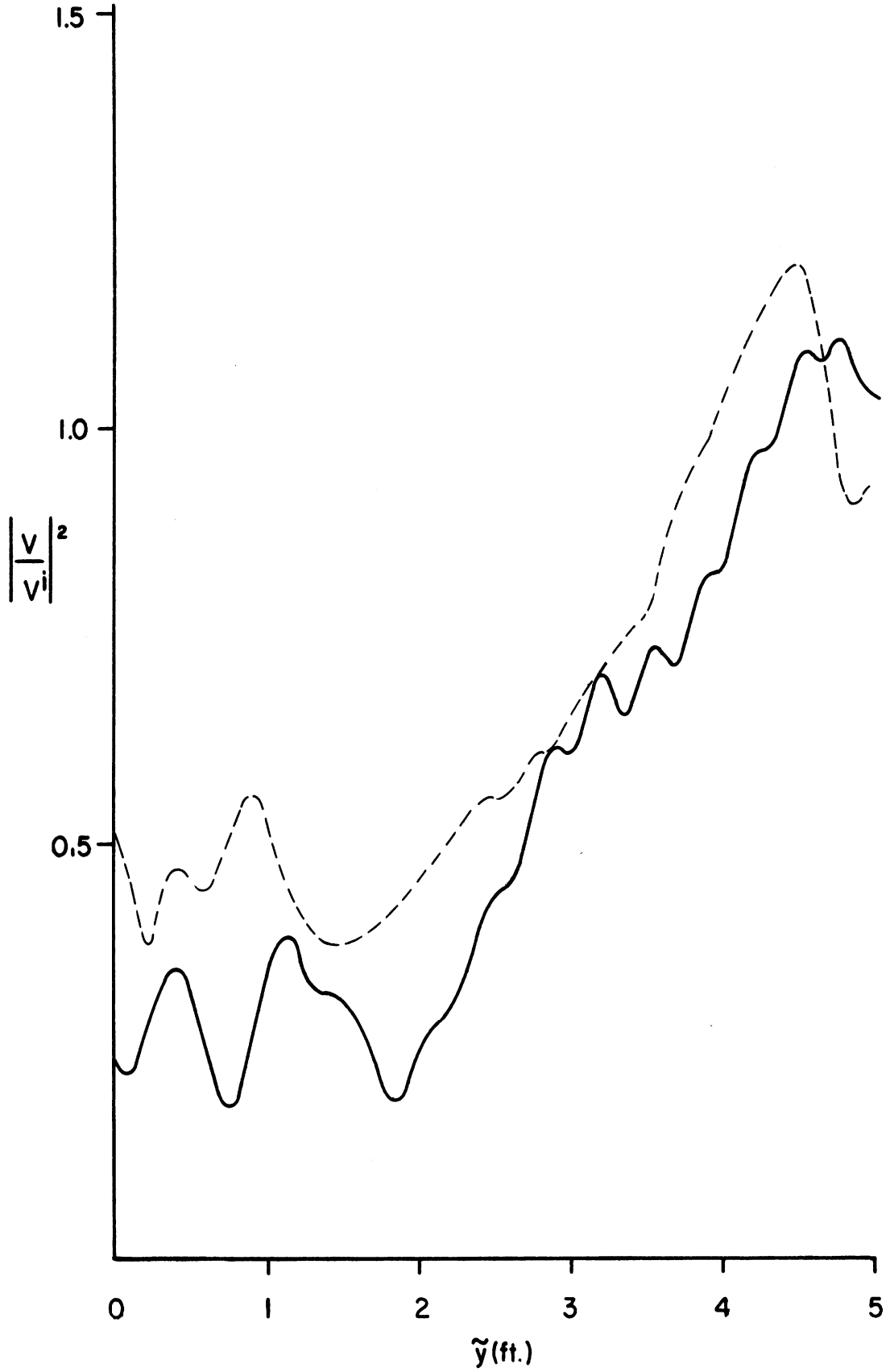

Fig. 24: Crawling man at 50 ft: --- 'average' experimental, —— theory for a = 3.3 ft. and b = 0.5 ft.

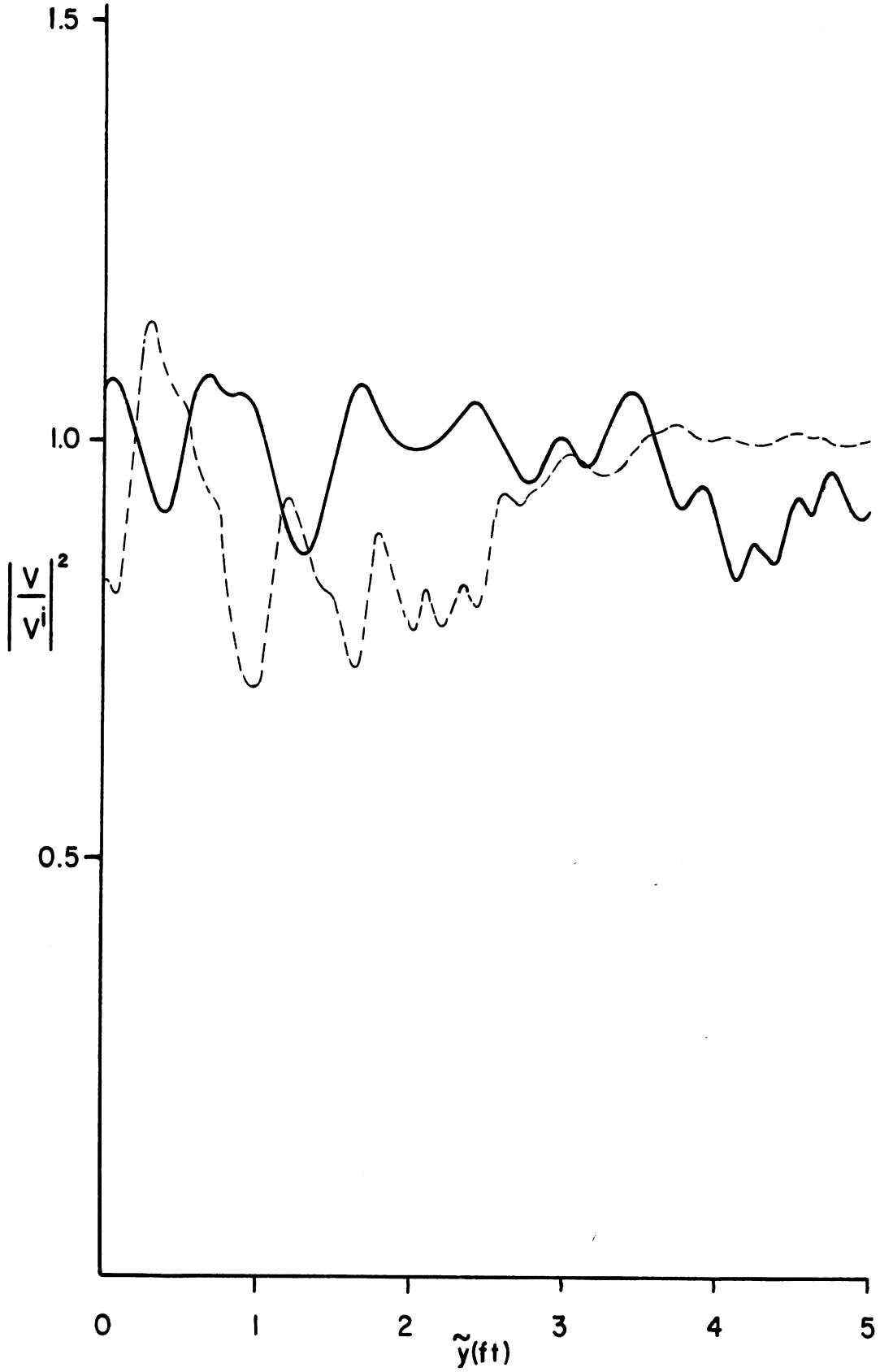

Fig. 25: Crawling man at 30 ft: --- 'average' experimental, —— theory for a = 3 ft. and b = 0.5 ft.

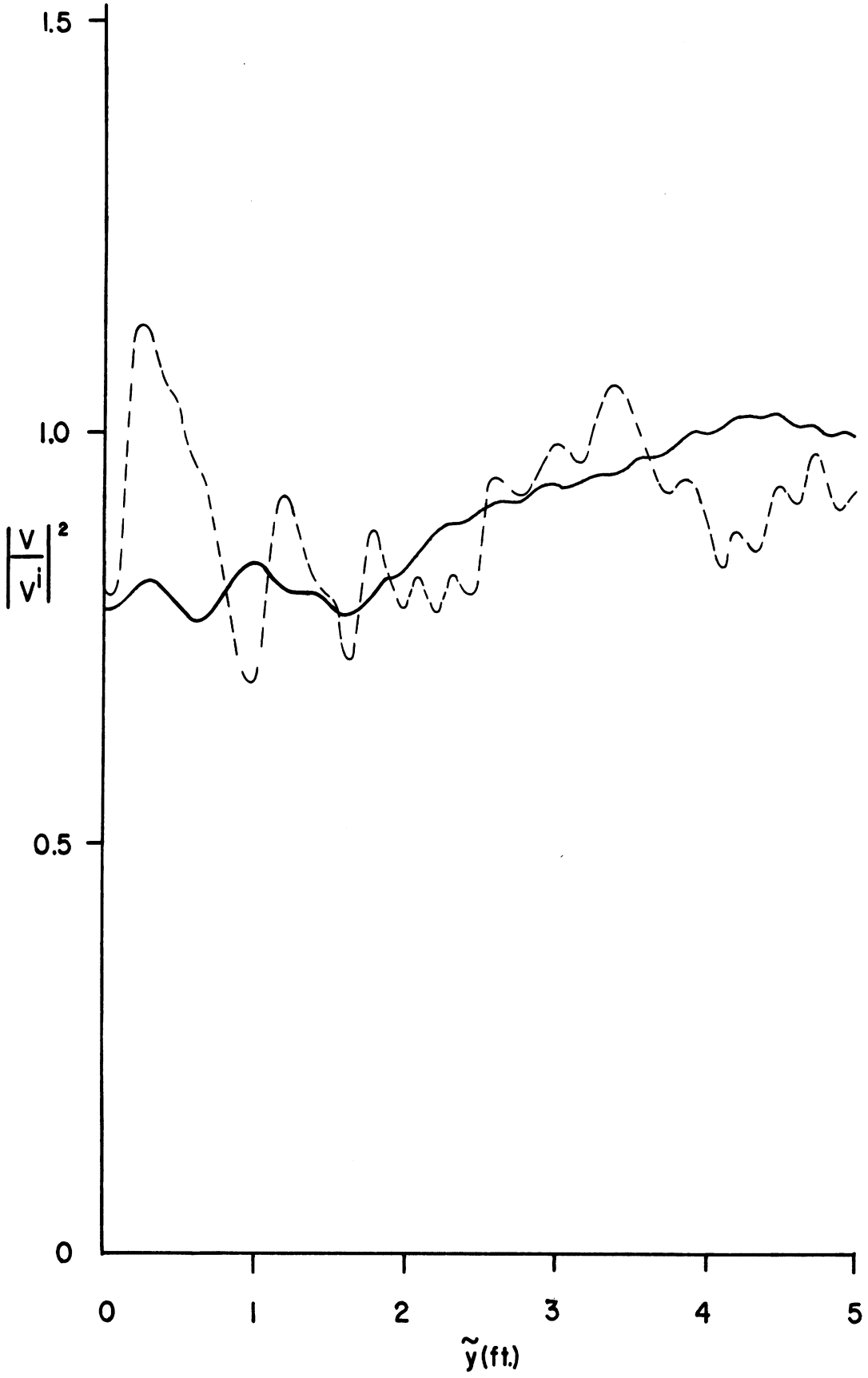

Fig. 26: Crawling man at 30 ft: --- 'average' experimental, —— theory for a = 3 ft. and b = 0.25 ft.

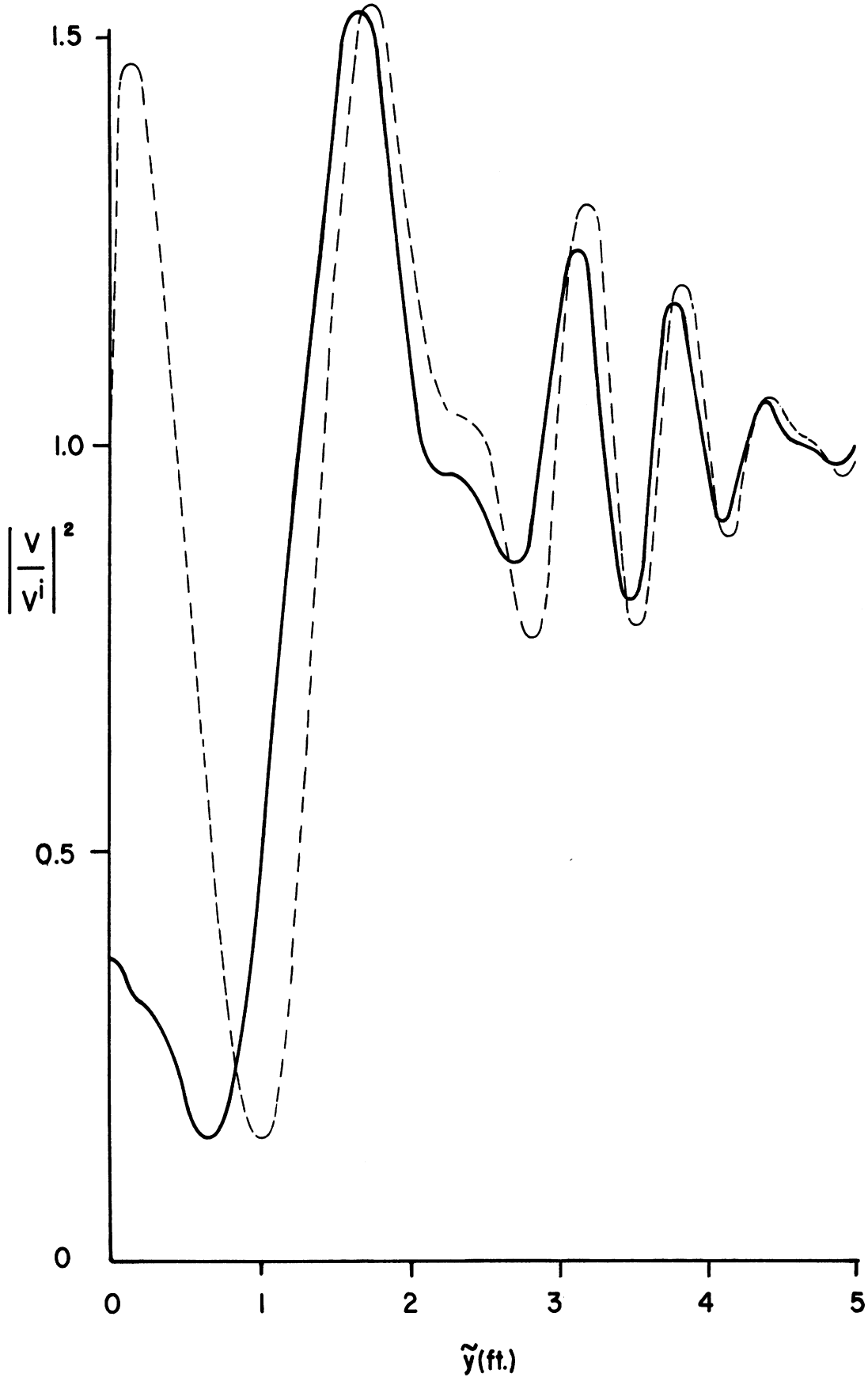

Fig. 27: Theoretical simulation of an erect man at 50 ft: —— in-phase ($z_1 = z_2 = 3.417$ ft.), --- phase quadrature ($z_1 = z_2 = 3.224$ ft.).

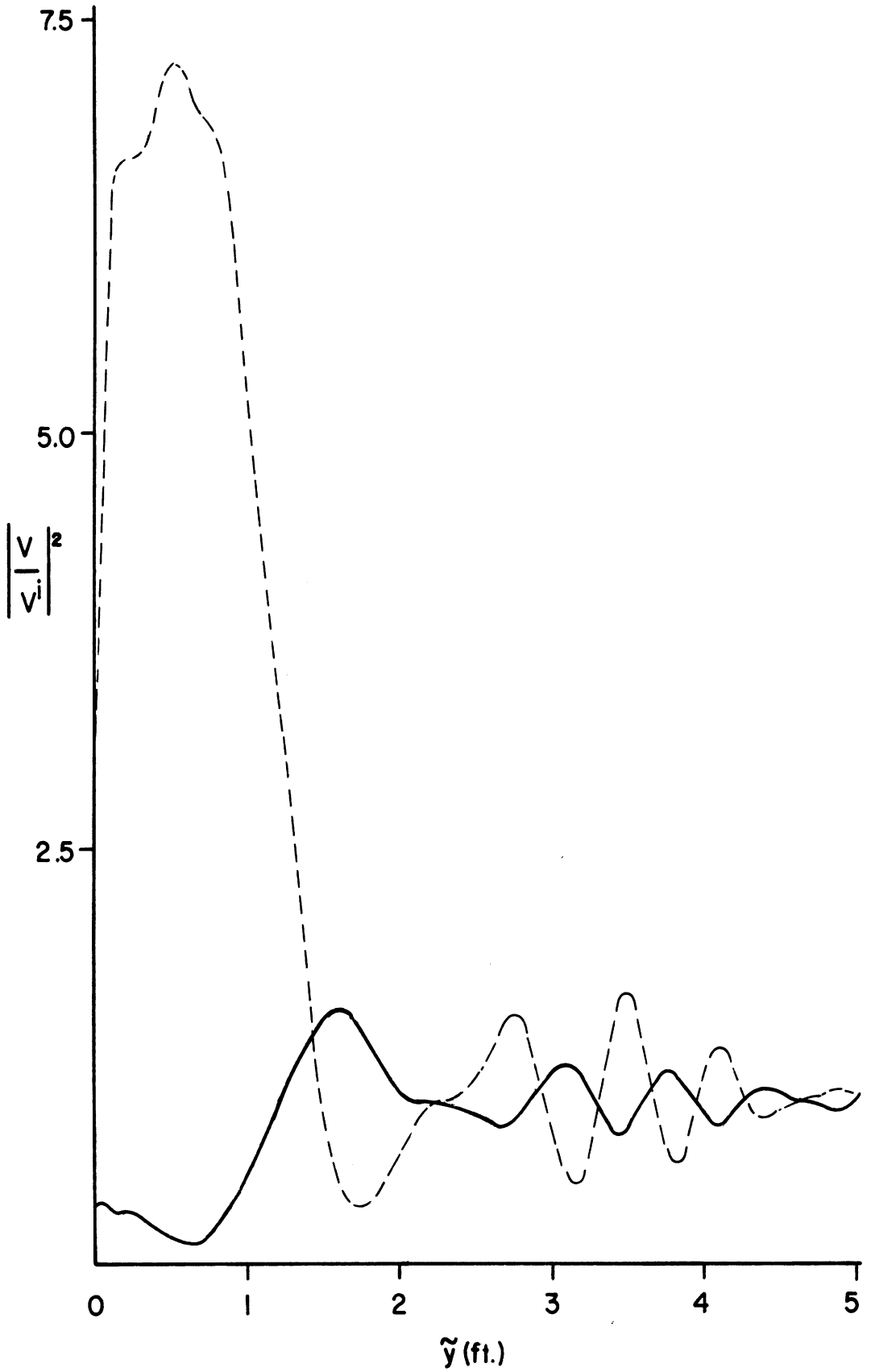

Fig. 28: Theoretical simulation of an erect man at 50 ft: —— in-phase ($z_1 = z_2 = 3.417$ ft.), --- out-of-phase ($z_1 = z_2 = 3.033$ ft.).

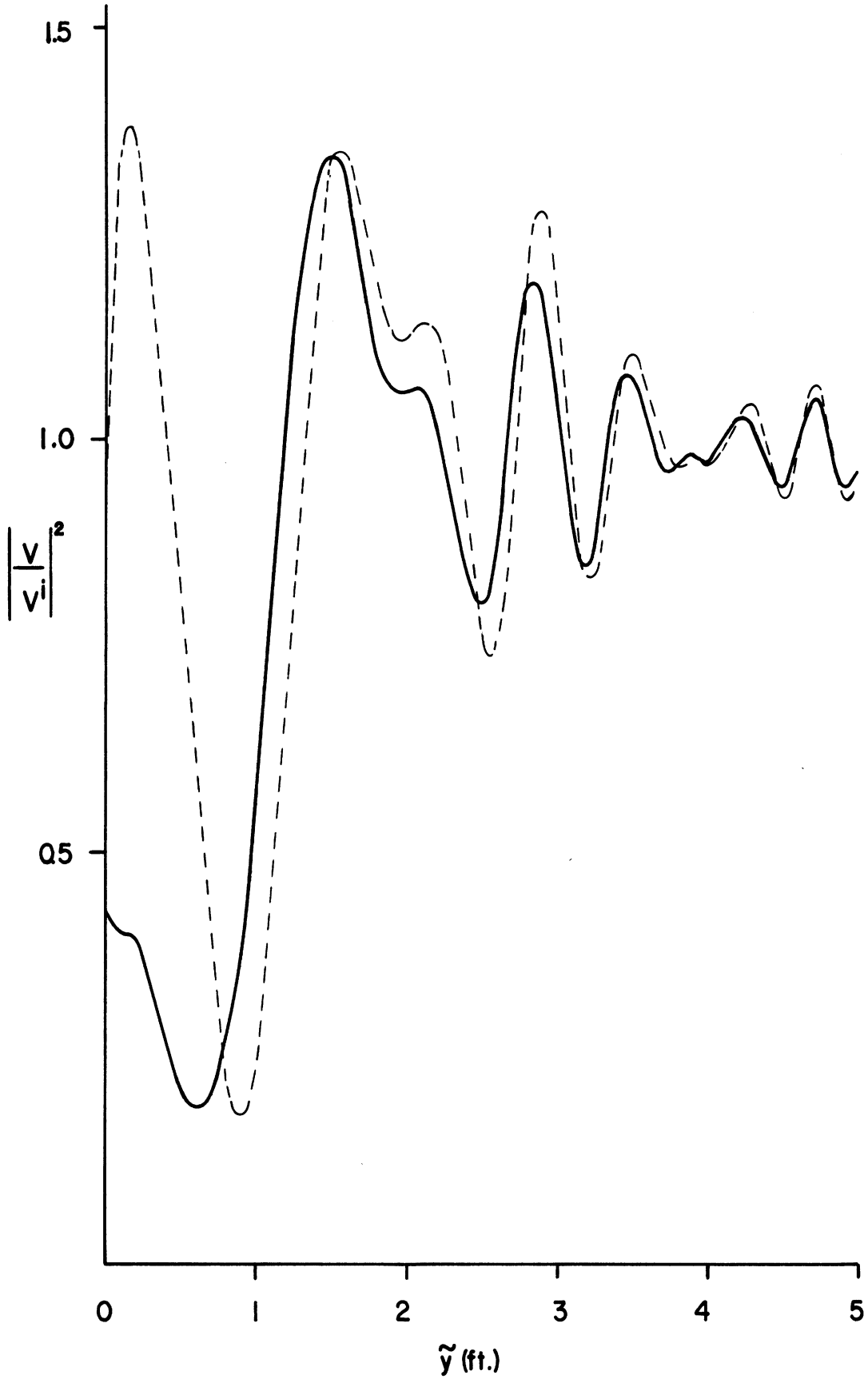

Fig. 29: Theoretical simulation of an erect man at 30 ft: —— in-phase ($z_1 = z_2 = 3.417$ ft.), --- phase quadrature ($z_1 = z_2 = 3.224$ ft.).

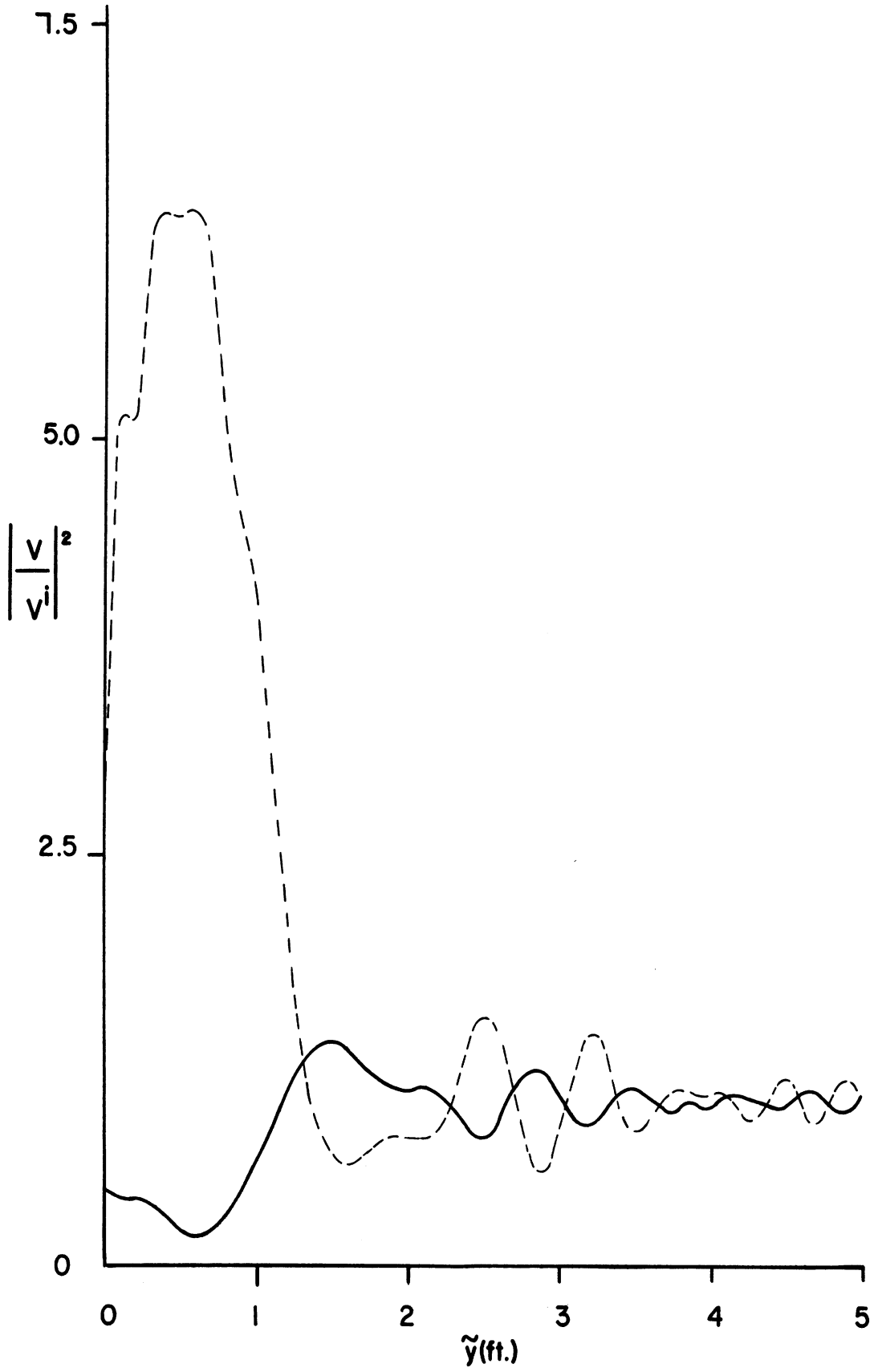

Fig. 30: Theoretical simulation of an erect man at 30 ft: —— in-phase ($z_1 = z_2 = 3.417$ ft.), --- out-of-phase ($z_1 = z_2 = 3.033$ ft.).

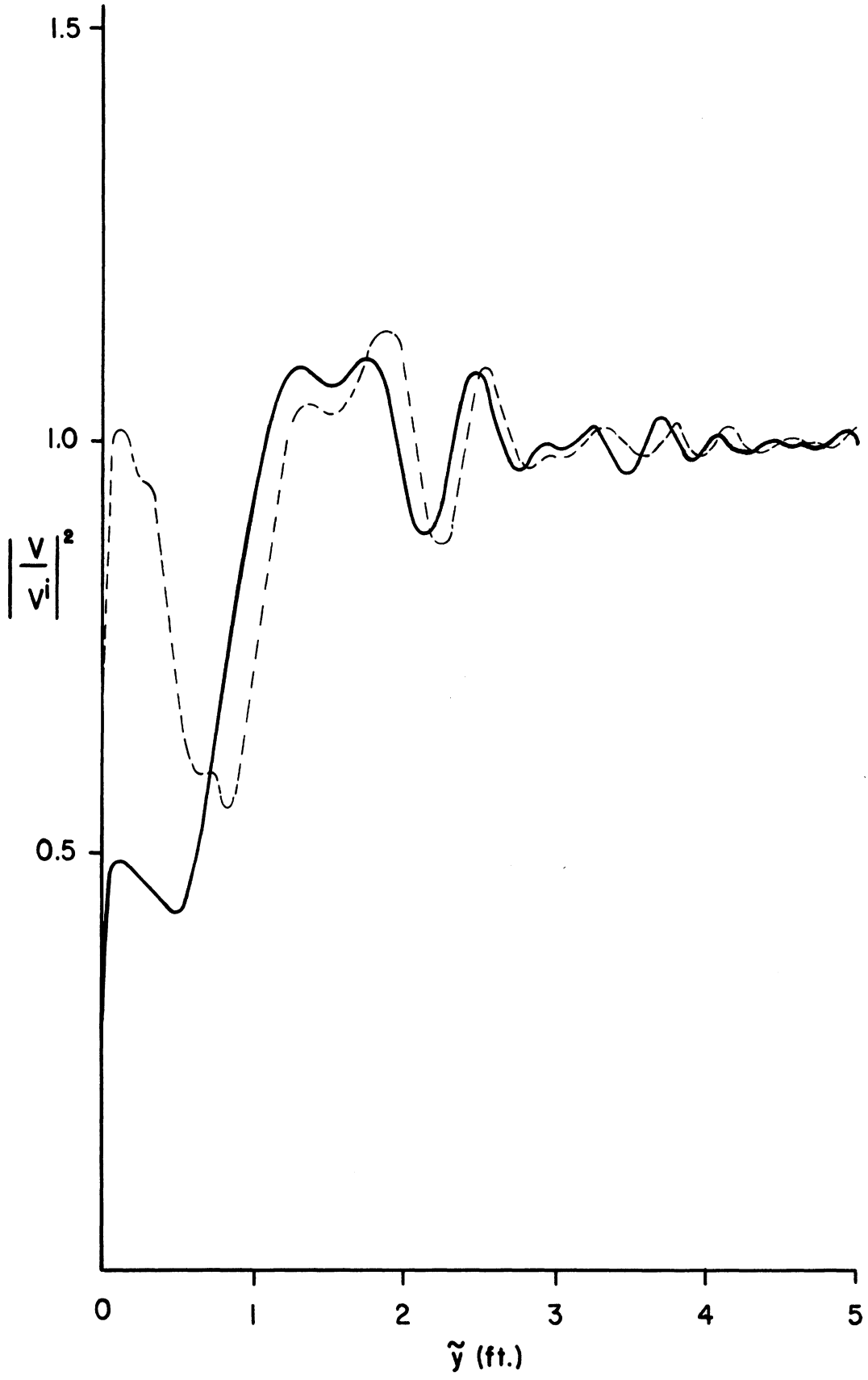

Fig. 31: Theoretical simulation of an erect man at 20 ft: —— in-phase ($z_1 = z_2 = 3.417$ ft.), --- phase quadrature ($z_1 = z_2 = 3.224$ ft.).

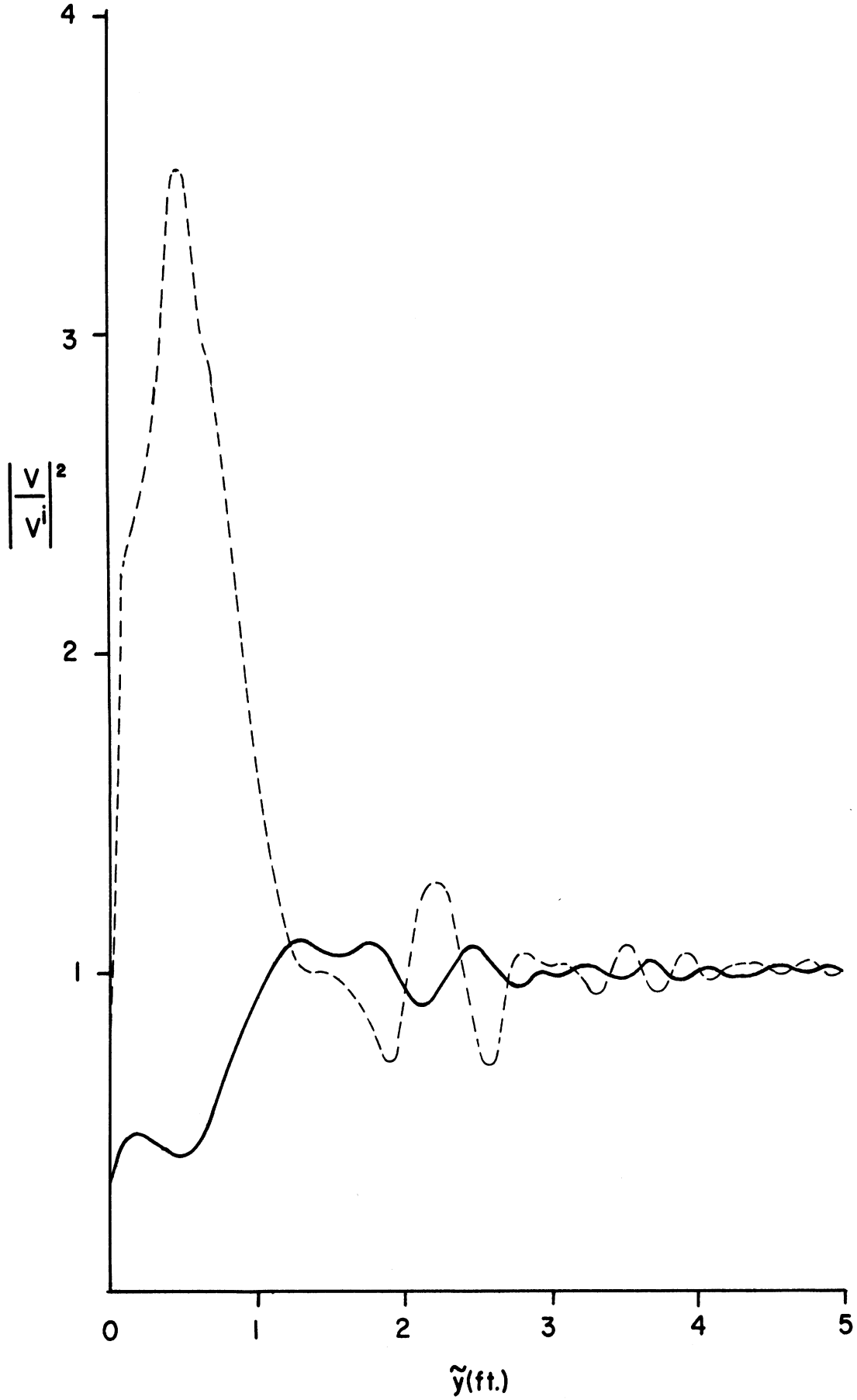

Fig. 32: Theoretical simulation of an erect man at 20 ft: —— in-phase ($z_1 = z_2 = 3.417$ ft.), --- out-of-phase ($z_1 = z_2 = 3.033$ ft.).

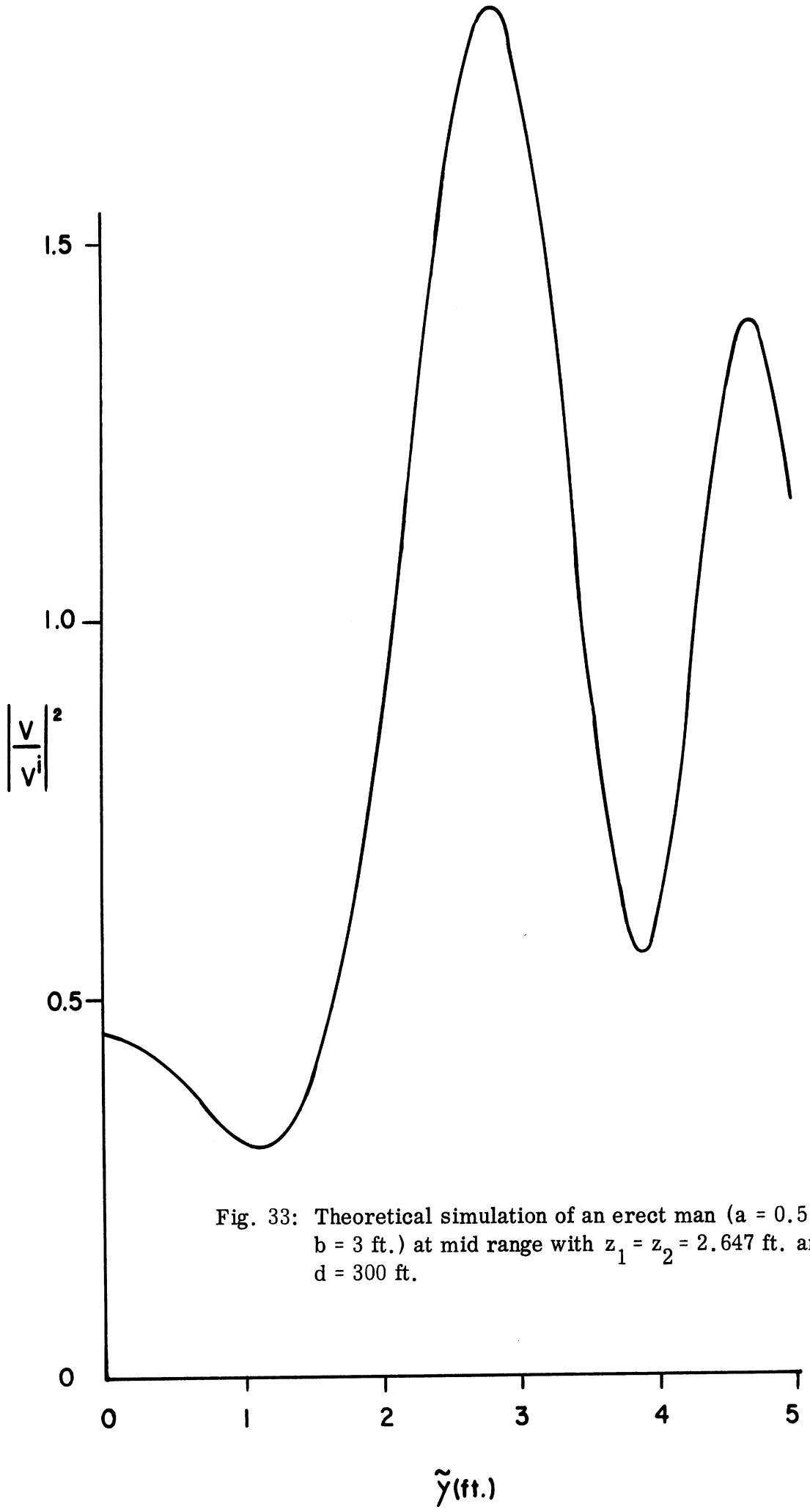

Fig. 33: Theoretical simulation of an erect man (a = 0.5 ft., b = 3 ft.) at mid range with $z_1 = z_2 = 2.647$ ft. and d = 300 ft.

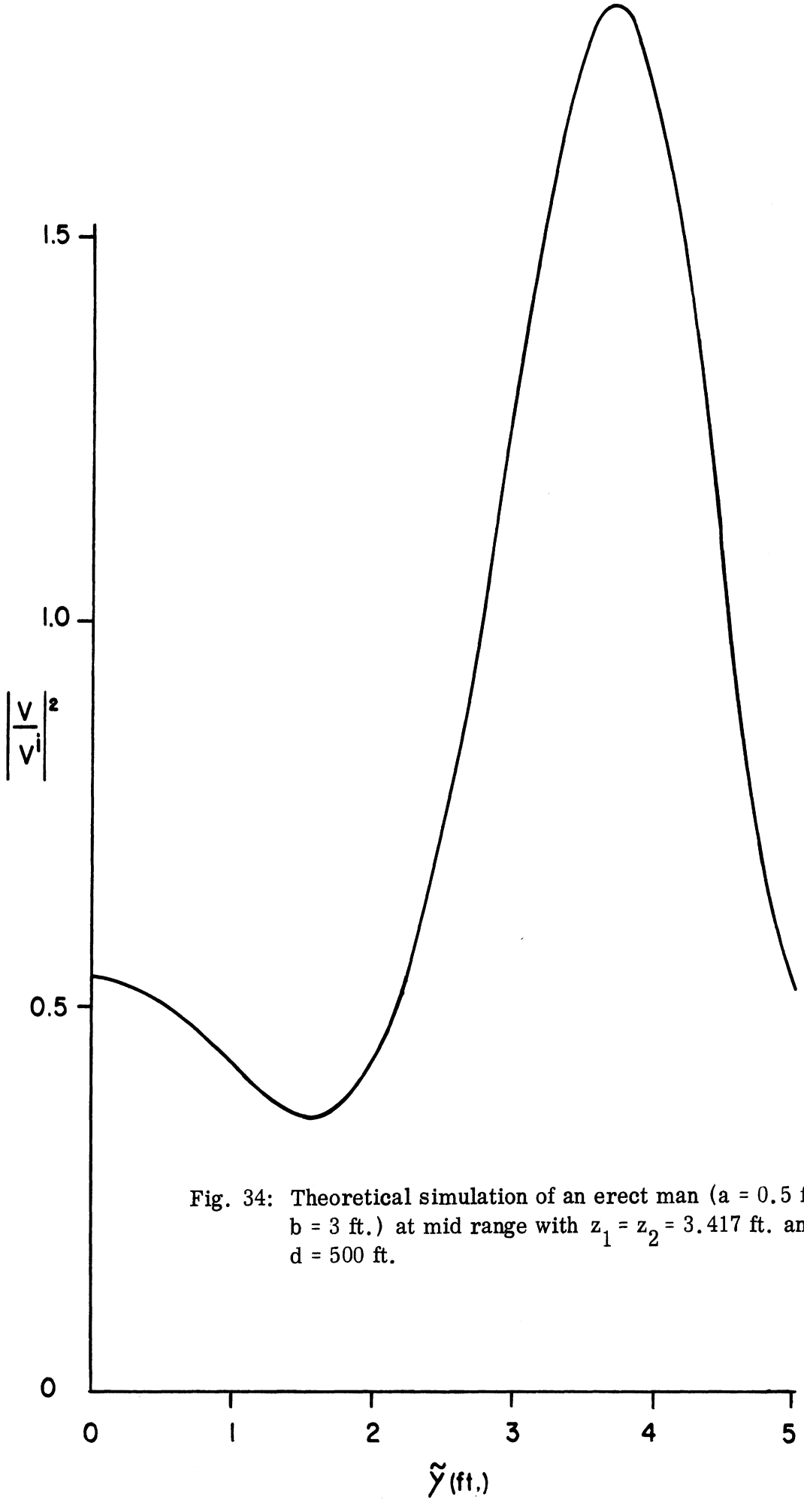

Fig. 34: Theoretical simulation of an erect man (a = 0.5 ft., b = 3 ft.) at mid range with $z_1 = z_2 = 3.417$ ft. and d = 500 ft.

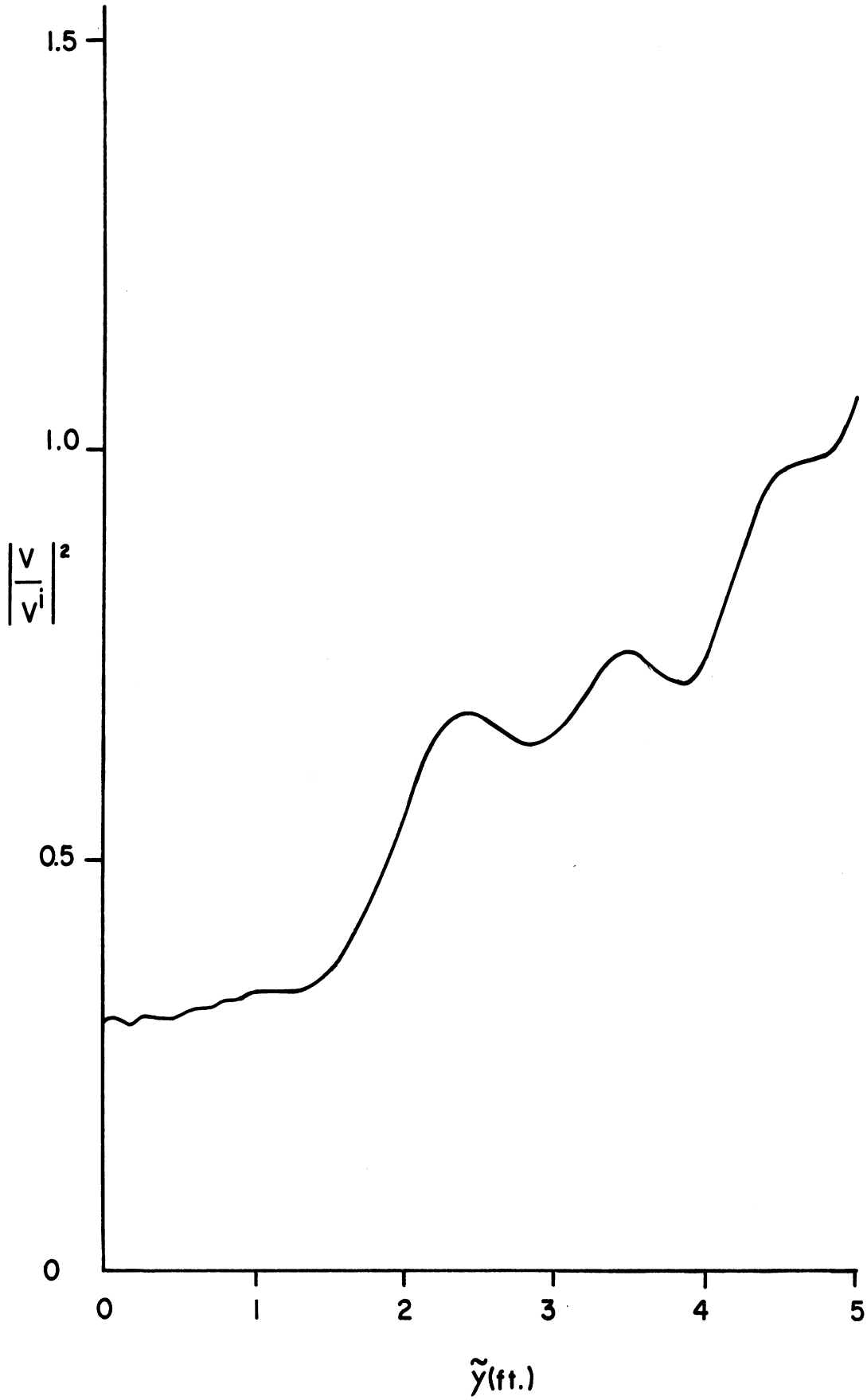

Fig. 35: Theoretical simulation of a crawling man (a = 3 ft., b = 0.5 ft.) at mid range with $z_1 = z_2 = 2.647$ ft. and d = 300 ft.

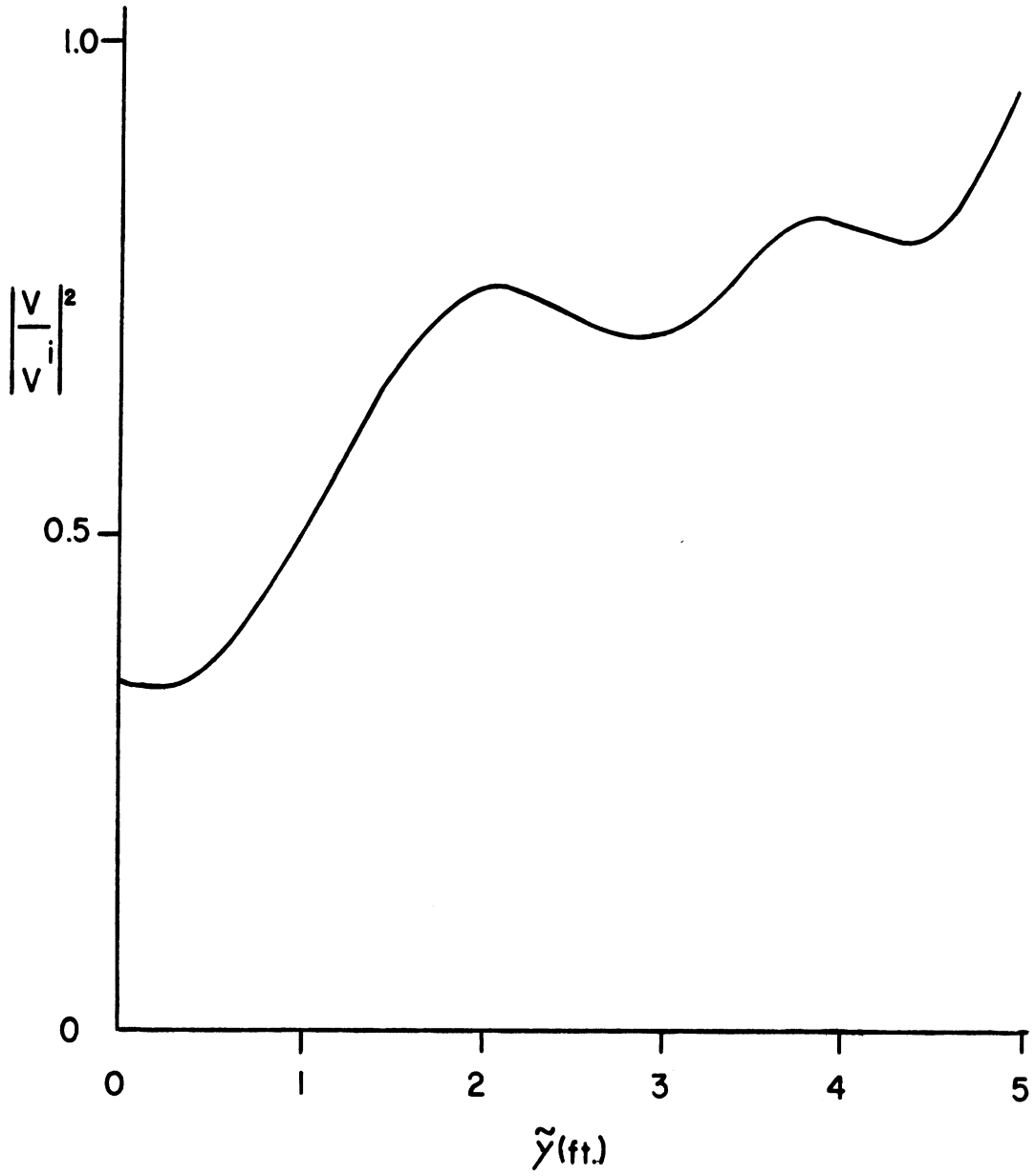

Fig. 36: Theoretical simulation of a crawling man (a = 3 ft., b = 0.5 ft.) at mid range with $z_1 = z_2 = 3.417$ ft. and d = 500 ft.

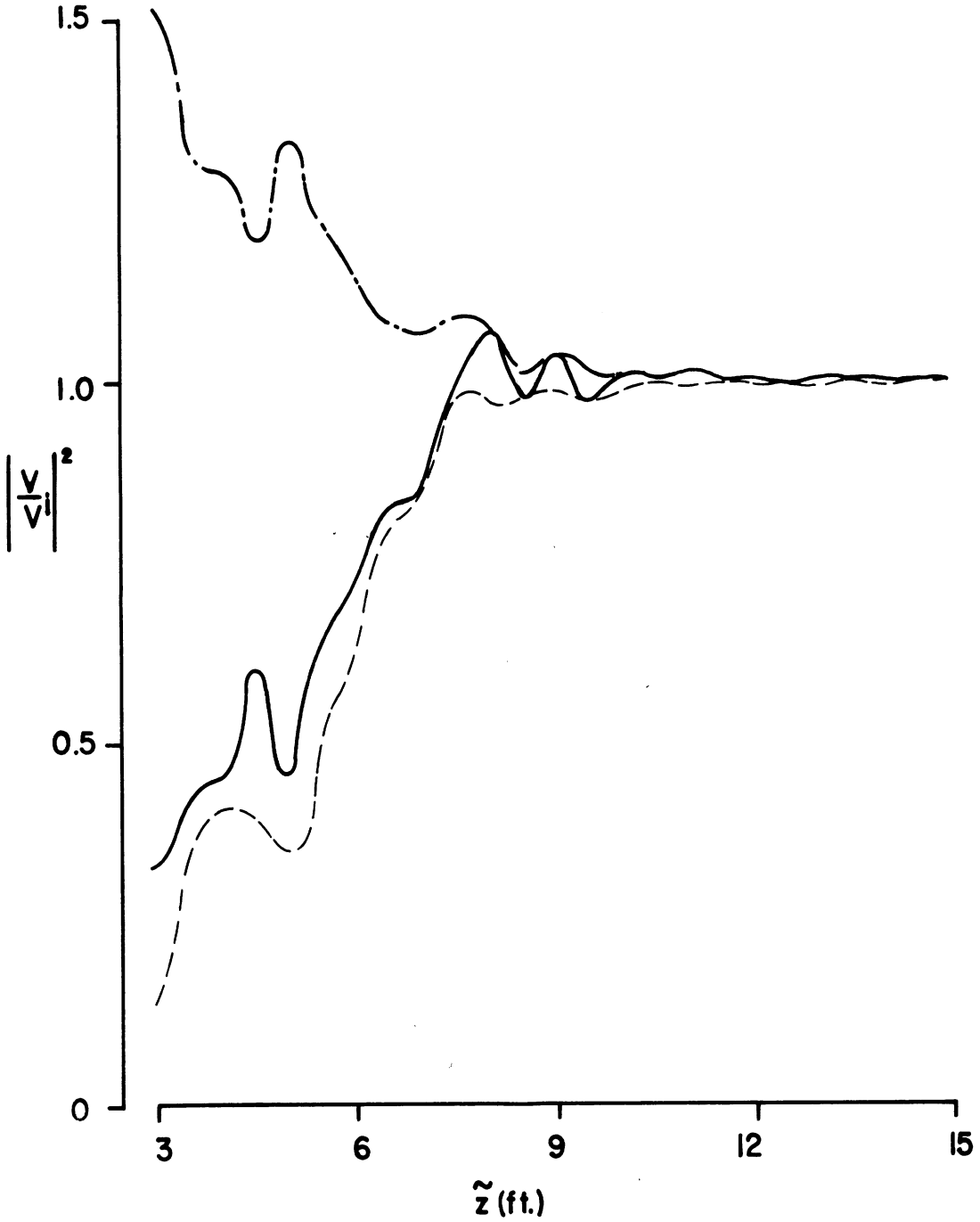

Fig. 37: Boresight (——), minimum (---) and maximum (—·—) values of the normalised power for a man (a = 0.5 ft., b = 3 ft.) crossing at d = 50 ft. as a function of his midpoint elevation $\tilde{z}$.

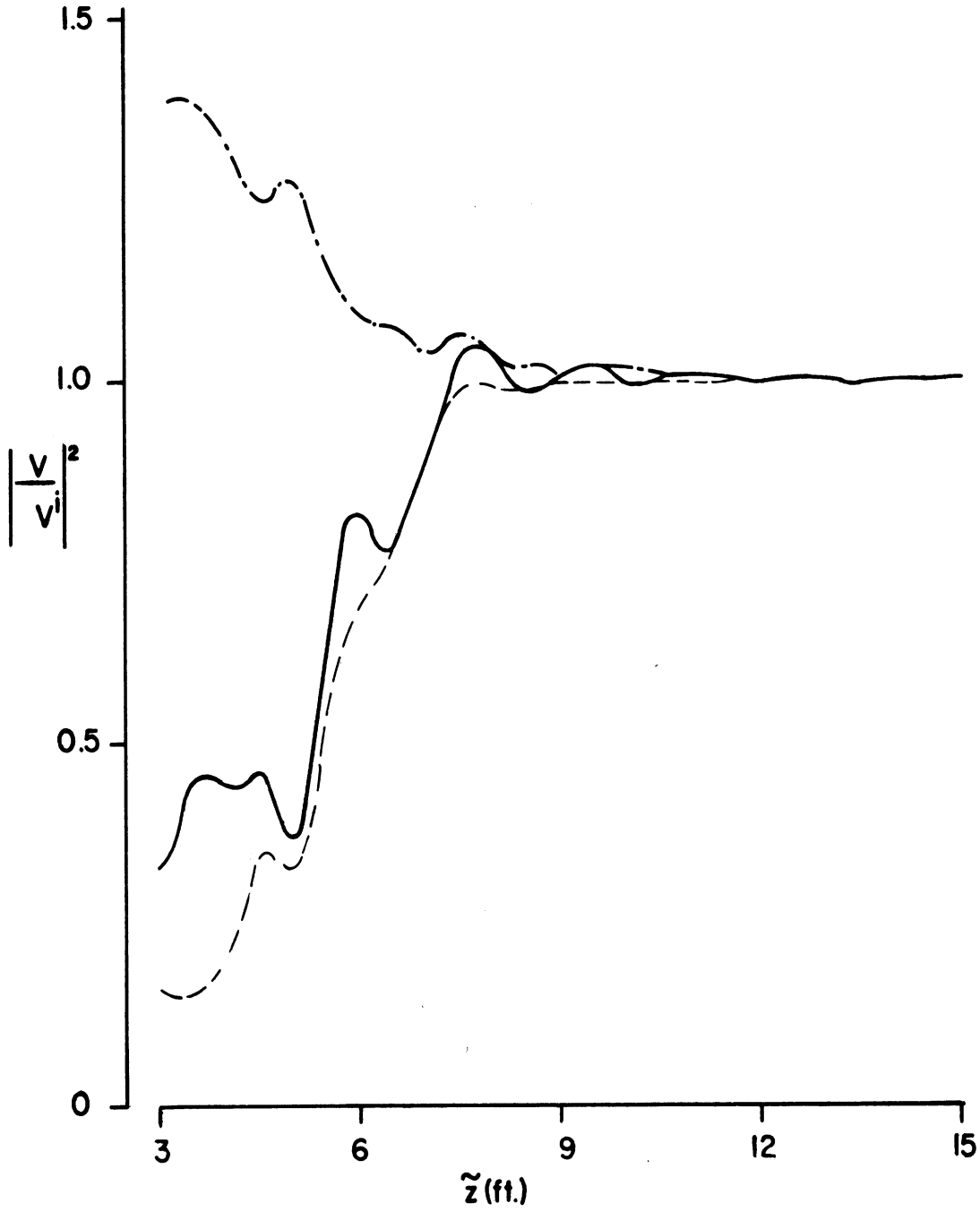

Fig. 38: Boresight (——), minimum (---) and maximum (— - —) values of the normalised power for a man (a = 0.5 ft., b = 3 ft.) crossing at d = 30 ft. as a function of his midpoint elevation $\tilde{z}$.

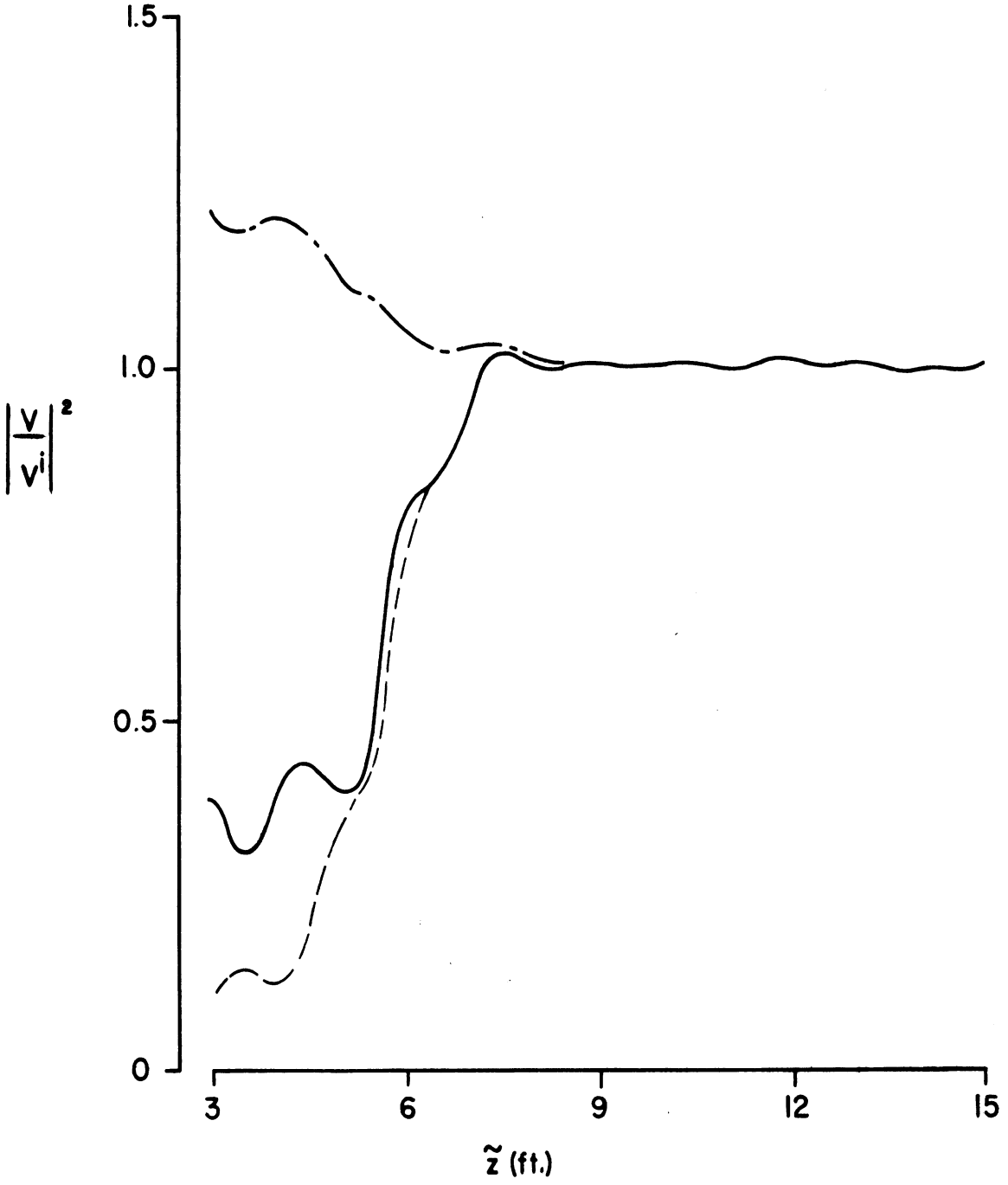

Fig. 39: Boresight (——), minimum (---) and maximum (—— - ——) values of the normalised power for a man (a = 0.5 ft., b = 3 ft.) crossing at d = 20 ft. as a function of his midpoint elevation $\tilde{z}$.

Acknowledgment

The author is indebted to Mr. T.J. Hart for his assistance with the computations.

References

Bowman, J.J., T.B.A. Senior and P.L.E. Uslenghi (1969), Electromagnetic and Acoustic Scattering by Simple Shapes, North Holland Publishing Company, Amsterdam.

Cosgriff, R.L., W.H. Peake and R.C. Taylor (1960), "Terrain scattering properties and sensor system design (Terrain Handbook II)", Eng. Exp. Sta. Bull. No. 181, The Ohio State University.

Janke, E. and F. Emde (1945), Tables of Functions with Formulae and Curves, Dover Publications, New York.

Row, R.V. and L.G. Abraham, Jr. (1965), "Analytical and experimental studies of the RF performance of the Sylvania Minuteman microwave anti-intrusion system", Sylvania Electronic Systems Appl. Res. Lab. Report No. 447.

Schultz, F.V., R.C. Burgener and S. King (1958), "Measurement of the radar cross section of a man", Proc. IRE 46(2), 476-481.

Stratton, J.A. (1941), Electromagnetic Theory, McGraw-Hill Book Co., Inc., New York.

```
      IMPLICIT REAL(K,I,M),COMPLEX(F)
    5 READ 300,RF,H1,H2,R,D,B,A,C,Y1,DELY,Y2,RHO,ARG
      ARG1=ARG*180./3.14159
      PRINT 100,R,RF,D,H1,B,H2,A,RHO,C,ARG1
      L=0
      K=6.283148*RF
      K2G=K/2./(D-D*D/R)
      FRFC=RHO*CMPLX(COS(ARG),SIN(ARG))
   ALPHA1=ATAN((H2-H1)/R)
      ALPHA2=ATAN((H2+H1)/R)
      RZ1=SQRT(R**2+(H2-H1)**2)
      RZ2=SQRT(R**2+(H2+H1)**2)
      PA1=POLAR(ALPHA1)
      PA2=POLAR(ALPHA2)
      GEPZ1=(H1*(R-D)+H2*D)/R
      GEPZ2=(H1*(D-R)+H2*D)/R
      FPHS1=CMPLX(COS(K*RZ1),SIN(K*RZ1))/RZ1
      FPHS2=CMPLX(COS(K*RZ2),SIN(K*RZ2))/RZ2
      FDIR=PA1**2*FPHS1+PA2**2*FPHS2*FRFC
      R2=REAL(FDIR)
      I2=AIMAG(FDIR)
      PRINT 101,R2,I2
      PRINT 105
   10 DELTA1=ATAN(SQRT((H1-C)**2+Y1**2)/D)
      DELTA2=ATAN(SQRT((H1+C)**2+Y1**2)/D)
      BETA1=ATAN(SQRT((H2-C)**2+Y1**2)/(R-D))
      BETA2=ATAN(SQRT((H2+C)**2+Y1**2)/(R-D))
      PD1=POLAR(DELTA1)
      PD2=POLAR(DELTA2)
      PB1=POLAR(BETA1)
      PB2=POLAR(BETA2)
      CALL CS(C1,S,K2G*(Y1+A)**2)
      F1=CMPLX(C1,S)
      CALL CS(C1,S,K2G*(Y1-A)**2)
      F2=CMPLX(C1,S)
      CALL CS(C1,S,K2G*(C-GEPZ1+B)**2)
      F3=CMPLX(C1,S)
      CALL CS(C1,S,K2G*(C-GEPZ1-B)**2)
      F4=CMPLX(C1,S)
      CALL CS(C1,S,K2G*(C+GEPZ1+B)**2)
      F5=CMPLX(C1,S)
      CALL CS(C1,S,K2G*(C+GEPZ1-B)**2)
      F6=CMPLX(C1,S)
      CALL CS(C1,S,K2G*(C-GEPZ2+B)**2)
      F7=CMPLX(C1,S)
      CALL CS(C1,S,K2G*(C-GEPZ2-B)**2)
      F8=CMPLX(C1,S)
      CALL CS(C1,S,K2G*(C+GEPZ2+B)**2)
      F9=CMPLX(C1,S)
      CALL CS(C1,S,K2G*(C+GEPZ2-B)**2)
      F10=CMPLX(C1,S)
      IF ((Y1+A).LT.0.) F1=-F1
      IF ((Y1-A).LT.0.) F2=-F2
      IF ((C-GEPZ1+B).LT.0.) F3=-F3
      IF ((C-GEPZ1-B).LT.0.) F4=-F4
      IF ((C+GEPZ1+B).LT.0.) F5=-F5
      IF ((C+GEPZ1-B).LT.0.) F6=-F6
      IF ((C-GEPZ2+B).LT.0.) F7=-F7
      IF ((C-GEPZ2-B).LT.0.) F8=-F8
      IF ((C+GEPZ2+B).LT.0.) F9=-F9
```

```
      IF ((C+GEPZ2-B).LT.0.) F10=-F10
      FSCAT=(0.,.5)*(F1-F2)*(FPHS1*(PD1*PB1*(F3-F4)+FRFC**2*PD2*PB2*(F5-
     )F6))+FRFC*FPHS2*(PD2*PB1*(F7-F8)+PD1*PB2*(F9-F10)))
      FVLTG=(FDIR+FSCAT)/FDIR
      MOD=CABS(FVLTG)**2
      R1=REAL(FDIR+FSCAT)
      I=AIMAG(FDIR+FSCAT)
      PRINT 102,Y1,R1,I,MOD
      Y1=Y1+DELY
      L=L+1
      IF(L.NE.41.AND.L.NE.91) GO TO 20
      PRINT 103
      PRINT 101,R2,I2
      PRINT 105
   20 IF(Y1.LE.Y2) GO TO 10
      GO TO 5
  100 FORMAT('1',20X,'PERTURBATION BY A MAN (OMNISPECTRA)'//3X,'RANGE',1
     )1X,'R (FT)',F8.3,10X,'FREQUENCY',6X,'F (GHZ)',F8.3/3X,'DISTANCE',8
     )X,'D (FT)',F8.3,10X,'TRANS HT',7X,'Z1 (FT)',F8.3/3X,'MODEL 1/2 HT'
     ),4X,'B (FT)',F8.3,10X,'REC HT',9X,'Z2 (FT)',F8.3/3X,'MODEL 1/2 WD'
     ),4X,'A (FT)',F8.3,10X,'RFLC COEF:   MAG      ',F8.3/3X,'CENTER HT'
     ),7X,'Z (FT)',F8.3,23X,'ARG (DEG)',F8.3//)
  101 FORMAT(' ',27X,'UNPERTURBED VOLTAGE'//25X,'REAL',16X,'IMAG'/16X,F1
     )4.5,7X,F14.5//)
  102 FORMAT('+',10X,F5.2,3F14.5/)
  103 FORMAT('1')
  105 FORMAT(' ',28X,'PERTURBED'/30X,'VOLTAGE',13X,'NORMALIZED'/14X,'Y',
     )10X,'REAL',10X,'IMAG',8X,'MOD SQRD'/)
  300 FORMAT(3F6.3,2F7.3,6F6.3,F4.2,F7.5)
      END
LE
```

PERTURBATION BY A MAN (OMNISPECTRA)

RANGE	R (FT)	100.000	FREQUENCY	F (GHZ)	10.525
DISTANCE	D (FT)	50.000	TRANS HT	Z1 (FT)	3.417
MODEL 1/2 HT	B (FT)	3.000	REC HT	Z2 (FT)	3.417
MODEL 1/2 WD	A (FT)	0.500	RFLC COEF:	MAG	0.950
CENTER HT	Z (FT)	3.000		ARG (DEG)	180.000

UNPERTURBED VOLTAGE

REAL	IMAG
0.01461	0.00806

Y	PERTURBED VOLTAGE REAL	PERTURBED VOLTAGE IMAG	NORMALIZED MOD SQRD
0.0	0.00319	0.00918	0.33935
0.10	0.00322	0.00903	0.32984
0.20	0.00330	0.00857	0.30297
0.30	0.00348	0.00783	0.26360
0.40	0.00380	0.00683	0.21970
0.50	0.00434	0.00564	0.18192
0.60	0.00516	0.00433	0.16281
0.70	0.00631	0.00301	0.17553
0.80	0.00783	0.00182	0.23186
0.90	0.00968	0.00093	0.33962
1.00	0.01179	0.00048	0.49988
1.10	0.01399	0.00061	0.70445
1.20	0.01607	0.00139	0.93467
1.30	0.01778	0.00276	1.16254
1.40	0.01888	0.00458	1.35483
1.50	0.01921	0.00656	1.48031
1.60	0.01878	0.00838	1.51872
1.70	0.01774	0.00971	1.46871
1.80	0.01640	0.01037	1.35124
1.90	0.01513	0.01033	1.20517
2.00	0.01425	0.00981	1.07465
2.10	0.01388	0.00913	0.99176
2.20	0.01391	0.00863	0.96236
2.30	0.01404	0.00844	0.96401
2.40	0.01401	0.00843	0.96053
2.50	0.01376	0.00832	0.92806
2.60	0.01351	0.00786	0.87695
2.70	0.01365	0.00713	0.85109
2.80	0.01439	0.00655	0.89753
2.90	0.01551	0.00664	1.02212
3.00	0.01633	0.00761	1.16595
3.10	0.01620	0.00899	1.23258
3.20	0.01501	0.00988	1.15965
3.30	0.01351	0.00955	0.98280
3.40	0.01281	0.00815	0.82762
3.50	0.01348	0.00674	0.81587
3.60	0.01498	0.00646	0.95577
3.70	0.01602	0.00749	1.12325
3.80	0.01574	0.00885	1.17071
3.90	0.01454	0.00928	1.06879
4.00	0.01367	0.00854	0.93267

UNPERTURBED VOLTAGE

REAL	IMAG
0.01461	0.00806

Y	PERTURBED VOLTAGE REAL	PERTURBED VOLTAGE IMAG	NORMALIZED MOD SQRD
4.10	0.01387	0.00756	0.89555
4.20	0.01469	0.00733	0.96755
4.30	0.01514	0.00785	1.04466
4.40	0.01492	0.00833	1.04878
4.50	0.01456	0.00832	1.01012
4.60	0.01449	0.00813	0.99183
4.70	0.01451	0.00810	0.99194
4.80	0.01443	0.00802	0.97900
4.90	0.01454	0.00779	0.97675
5.00	0.01491	0.00784	1.01916